SEDIMENT-RICH MELTWATER PLUMES AND ICE-PROXIMAL FANS AT THE MARGINS OF MODERN AND ANCIENT TIDEWATER GLACIERS: OBSERVATIONS AND MODELLING

J.A. DOWDESWELL[1], K.A. HOGAN[1,*], N.S. ARNOLD[1], R.I. MUGFORD[1,*], M. WELLS[2] J.P.P. HIRST[2] and C. DECALF[2]

[1]Scott Polar Research Institute, University of Cambridge, Cambridge CB2 1ER, UK

[2]BP Exploration, Chertsey Road, Sunbury-on-Thames, Middlesex TW16 7LN, UK

[*]Now at British Antarctic Survey, High Cross, Madingley Road, Cambridge CB3 0ET, UK

ABSTRACT

Turbid meltwater plumes and ice-proximal fans occur where subglacial streams reach the grounded marine margins of modern and ancient tidewater glaciers. However, the spacing and temporal stability of these subglacial channels is poorly understood. This has significant implications for understanding the geometry and distribution of Quaternary and ancient ice-proximal fans that can form important aquifers and hydrocarbon reservoirs. Remote-sensing and numerical-modelling techniques are applied to the 200 km-long marine margin of a Svalbard ice cap, Austfonna, to quantify turbid meltwater-plume distribution and predict its temporal stability. Results are combined with observations from geophysical data close to the modern ice front to refine existing depositional models for ice-proximal fans. Plumes are spaced about 3 km apart and their distribution along the ice front is stable over decades. Numerical modelling also predicts the drainage pattern and meltwater discharge beneath the ice cap; modelled water-routing patterns are in reasonable agreement with satellite-mapped plume locations. However, glacial retreat of several kilometres over the past 40 years has limited build-up of significant ice-proximal fans. A single fan and moraine ridge is noted from marine-geophysical surveys. Closer to the ice front there are smaller recessional moraines and polygonal sediment lobes but no identifiable fans. Schematic models of ice-proximal deposits represent varying glacier-terminus stability: (i) stable terminus where meltwater sedimentation produces an ice-proximal fan; (ii) quasi-stable terminus, where glacier readvance pushes or thrusts up ice-proximal deposits into a morainal bank; (iii) retreating terminus, with short still-stands, allowing only small sediment lobes to build up at melt-stream portals. These modern investigations are complemented with outcrop and subsurface observations and numerical modelling of an ancient, Ordovician glacial system. Thick turbidite successions and large fans in the Late Ordovician suggest either high-magnitude events or sustained high discharge, consistent with a relatively mild palaeo-glacial setting.

INTRODUCTION

When subglacial meltwater streams reach the grounded marine margins of tidewater glaciers and ice caps, fresh water normally rises to produce readily identifiable surface plumes of turbid meltwater (e.g. Syvitski, 1989; Powell, 1990; Mugford and Dowdeswell, 2011); only occasionally is the water dense enough to form turbid underflows (e.g. Mulder and Syvitski, 2005). Sedimentation at melt-stream portals at the base of tidewater glacier

terminal ice cliffs is usually characterised by the formation of ice-proximal fans close to the grounding-line (Powell, 1990; Powell and Domack, 1995; Seramur et al., 1997). Deposition of the coarse-fraction takes place close to the point-sources provided by subglacial channel mouths, linked to rapid initial energy loss. The finer sands, silts and clays are deposited progressively further from the portal by rain-out from suspension. However, the distribution of subglacial channels at the margins of modern marine-terminating ice masses is not well known. Questions regarding the spacing of channel mouths along tidewater ice margins, and the stability of such margins over decades remain. Quantifying the distribution pattern of subglacial channel mouths along a modern ice margin provides important constraints on the likely development and distribution of ice-proximal fans in both the Quaternary and longer-term geological record. Glacial meltwater channels, with their associated sandy fill and relatively coarse-grained ice-marginal fans, have also been reported from ancient glacial-sedimentary systems (e.g. Koch and Isbell, 2013) and form important reservoir rocks for hydrocarbons in, for example, the Late Ordovician glacial rocks of Northern Africa (e.g. Hirst, 2012).

The 200 km-long open-marine margin of the Austfonna ice cap in eastern Svalbard is the longest continuous tidewater glacier terminus in the Arctic today (Fig. 1A) (Dowdeswell, 1986). These ice cliffs, combined with existing glaciological data on ice-cap form, flow and mass balance (Dowdeswell et al., 1986, 2008; Hagen et al., 2003; Schuler et al., 2007), make Austfonna a very suitable location to measure and model meltwater-plume behaviour and the resulting pattern of glacimarine sedimentation. The 8,000 km^2 ice cap has a maximum ice thickness of 560 m and a total volume of about 2,500 km^3. Just under 30%, some 2,300 km^2 of its area, lies below present sea level, mainly inland of the extensive tidewater ice cliffs on its eastern side (Dowdeswell et al., 1986; Dowdeswell, 1989). Marine-geophysical observations of the adjacent sea-floor record the nature of submarine landforms and sediments (Solheim and Pfirman, 1985; Solheim, 1991; Robinson and Dowdeswell, 2011), and plumes of suspended sediment are known to emanate from melt streams draining to the ice-cap terminus (Pfirman and Solheim, 1989). 60 MHz ice-penetrating radar records provide measurements of the ice thickness of Austfonna; combined with surface-elevation data, they yield the digital-elevation models (DEMs) of the ice-cap surface and bed used in numerical modelling (Dowdeswell et al., 1986, 2008).

In this paper, digital Landsat satellite imagery from 1976 to 2012 is analysed to record the time-dependent behaviour of suspended-sediment plumes that represent the mouths of active subglacial channels at the marginal ice cliffs of Austfonna. Numerical modelling is used to

calculate ice-cap basal water-pressure gradients and to predict the distribution of subglacial channels. Model predictions of turbid-plume locations are then tested against the satellite-observed distribution of turbid plumes. A second numerical model, of the fluid dynamics of turbid plume flow-behaviour, is then used to predict plume and ice-proximal fan extent and the volume and rate of associated glacimarine deposition. These results are combined with swath-bathymetric, shallow-acoustic and sediment-core data from offshore of Austfonna (Fig. 1B), to characterise recent ice-proximal glacimarine sedimentation. Schematic models of modern and ancient tidewater glacier ice-proximal fans are constructed, based on a combination of field observations and numerical-model predictions; evidence comes from both offshore of Austfonna today and from the ancient Late Ordovician rocks of the Illizi Basin, Algeria. Finally, the numerical ice-sheet and water-pressure model is used to generate predictions of how broad-scale subglacial meltwater drainage patterns link to the presence or otherwise of ice streams in an ancient pre-Quaternary glacial system, given assumptions on the climatology and glaciology of the Late Ordovician North African ice sheet.

SATELLITE OBSERVATIONS: TURBID MELTWATER PLUME LOCATIONS

Analysis of Landsat satellite data

Examples of sediment-rich meltwater plumes in the waters immediately east of Austfonna are shown in Figures 2 and 3. Available cloud-free summer (July-September) Landsat (Multi-Spectral Scanner, MSS; Thematic Mapper, TM; and Enhanced Thematic Mapper, ETM+) images , with open water rather than a sea-ice cover along the ice-cap front, were collated and indexed for plume identification. Image processing and plume mapping methods are summarised here and in Figure 2A. More than 120 images were processed, resulting in mapped meltwater plume locations for 42 dates from 16 different years between 1976 and 2012 (Fig. 4A). Specific Landsat bands are known to aid identification of suspended sediments in water (e.g. Pfirman and Solheim, 1989) and, typically, band combinations of 2-3-4 (wavelengths: 0.525-0.605 μm, 0.63-0.69 μm, 0.76-0.90 μm, respectively) or 1-2-3 (wavelengths: 0.45-0.515 μm, 0.525-0.605 μm, 0.63-0.69 μm) were used for plume mapping. Image enhancement techniques, including contrast stretching, were also used to highlight plumes on optical imagery. Plumes were manually delineated as a line or "gate" along the ice margin denoting the width of a given plume in Geographical Information System (GIS) software. All mapped plumes were then collated into a master file (Figs. 3A, 4). Identification of individual plumes was most reliable early in the melt season, before significant volumes of sediment had been released in the offshore zone. Later in the melt season, sediment-laden

meltwater is often transported along the ice margin by coastal currents, making plume "gates" more difficult to identify. Other problems in obtaining spatial and temporal information on plume locations included the presence of sea-ice and icebergs early and late in the melt season, and the tendency for Austfonna to be covered by clouds.

In the master plume file (Fig. 4A), all plume locations were assigned an ID number (from Bråsvelbreen (Basin 1) in the southwest to Leighbreen (Basin 10) in the north; Fig. 3A). 58 plume locations were identified from data with a spatial resolution of 80 m for Landsat MSS images or 30 m for TM and ETM+ images (Fig. 4). The master file was then used to assign a numeric code of "plume status" to each plume location: absent (0), present (1), probable (2), obscured (3) (by sediment-laden water from adjacent plumes, clouds and/or icebergs and sea ice), and no data (4) (Figs. 2, 4). No attempt was made to quantify the flux of suspended sediment, for two reasons; first, our main aim was to define presence or absence and, hence, the spatial distribution of melt-stream portals; secondly, it is difficult to convert Landsat relative-brightness values into quantitative radiance measurements and considerable field calibration (unavailable for Austfonna) is required to calculate absolute values of suspended-sediment concentration (e.g. Chu et al., 2012; Rees, 2013).

Turbid meltwater plume locations from satellite imagery

The distribution of turbid meltwater plumes east of Austfonna is shown in Figure 3A. The recurrence of plumes at each location is quantified in Figure 4. Average plume spacing along the entire margin is about 3 km, but can be as little as 400 m or as much as 7 km. Relatively few meltwater plumes were mapped in the southernmost basins (1, 2 and part of 3) and also in the northernmost basin (10; Fig. 3A). Of note is the absence of plumes emanating from the marine margin of Bråsvellbreen (Basin 1). Bråsvellbreen is well-known as a surge-type glacier that advanced some 20 km along a 30-km-wide front in the 1930s (Schytt, 1969; Dowdeswell, 1986; Solheim, 1991). Recent aerial photographs show significant meltwater on the surface of Bråsvellbreen, as supraglacial lakes and well-defined meltwater streams. Supraglacial water flow appears to be the main drainage route for meltwater for this basin at present, given that much of its surface is stagnant and free of crevasses during the quiescent phase of the surge cycle.

There is a clear increase in meltwater-plumes density in the northern part of Basin 3 and at the margins of Basins 4-6 relative to other parts of the ice margin of Austfonna (Fig. 3). Here, average plume spacing for all mapped plumes is around 2 km. However, it is important to stress that not all these plumes were necessarily active concurrently (see Plumes 9-39, Fig.

4A). in addition, several of the largest plumes are consistent major conduits for subglacial meltwater and sediment transfer (e.g. Plumes 1, 5, 17, 24, 36, 38, Fig. 4). In Basins 1-3, major meltwater plumes occur close to the boundaries with adjacent glacier drainage basins, suggesting that the edges of glaciological drainage basins can act as major pathways for subglacial meltwater. Given that the centre of a glacial trough is likely to be occupied by the thickest ice, subglacial-drainage theory would explain the preferential occurrence of melt streams close to basin boundaries because basal water-hydraulic potential gradients are likely to cause subglacial water routing towards the edges of a trough (Shreve, 1972; Arnold et al., 1998).

SATELLITE OBSERVATIONS: ICE MARGIN STABILITY

Analysis of Landsat satellite data

A number of digital satellite images of Austfonna acquired between 1973 and 2012 were used to give approximately decadal snapshots of marine ice-marginal position (Fig. 5). Images were obtained by the Landsat MSS, TM, ETM+ and Advanced Spaceborne Thermal Emission and Reflection Radiometer (ASTER) systems.

Stability of the tidewater margin of Austfonna

The tidewater ice cliffs at the marine margins of Austfonna have typically retreated by several kilometres over the past 40 years (Fig. 5), although there are variations in retreat between individual ice-cap basins (Fig. 5E). Retreat has been relatively consistent between the four approximately ten-year intervals. Note that parts of the margins of Basins 3 and 4 underwent speed-up and minor readvance in the early 1990s (Dowdeswell et al., 1999) and again since 2012 (McMillan et al., Submitted). Semi-continuous retreat, except where surge-type glaciers are active (Meier and Post, 1969), is typical of most tidewater glaciers in Svalbard (e.g. Dowdeswell et al., 1997; Hagen et al., 2003; Błaszczyk et al., 2013). However, detailed observations from other Svalbard tidewater glaciers suggest that, in any given year, terminus retreat takes place mainly during summer when mass loss by iceberg calving is at a maximum, and that minor readvances may characterise winter periods when iceberg production is largely supressed due to the presence of shorefast sea-ice in many fjords (Dowdeswell, 1989; Ottesen and Dowdeswell, 2006). Iceberg production tends to increase with water depth, due to increasing marginal buoyancy (e.g. Pelto and Warren, 1991; Benn et al., 2007). Thus, with other ice-dynamics factors held constant, ice margins grounded in relatively shallow water are likely to be more stable than grounding-lines at greater depths.

These findings on tidewater glacier terminus fluctuations at Austfonna, and the more general retreat of glaciers worldwide (e.g. Cook et al., 2005; Barry, 2006), suggest that, in terms of ice-margin position, a stable location for subglacial melt stream portals may be the exception rather than the norm at both decadal and annual timescales. Whereas stream-portal position and spacing may not vary greatly along a tidewater ice front (Fig. 4), small winter readvances superimposed upon more general terminus retreat may mean that instability in the location of a given portal resulting from retreat/advance of the ice front is a major constraint on sediment build-up to form ice-proximal fans, unless the rate of sedimentation is particularly high. Thus, the development of clearly identifiable fans is more likely for those tidewater ice margins that are relatively stable over years to decades. The observed build-up of an ice-proximal fan at the margins of Muir Glacier in south-east Alaska, for example, took place specifically when the ice-terminus position was relatively stable for a period of about 20 years (Seramur et al., 1997).

MODEL PREDICTIONS OF SUBGLACIAL DRAINAGE PATTERNS AND MELTWATER PLUME LOCATIONS

Numerical-modelling can also be used to predict the drainage pattern and time-dependent discharge of meltwater beneath Austfonna and, hence, the likely spacing of ice-proximal fans beyond its margins. This water-routing model used requires, in turn, input from an ice-cap surface-melt model. Predictions from the water-routing model can then be tested using the satellite-observed locations of turbid plumes beyond Austfonna (Fig. 4).

Calculations of meltwater production and discharge on Austfonna

The time-dependent flux of meltwater feeding the subglacial drainage system of Austfonna is derived by routing calculated surface melt down a subglacial hydraulic potential surface. Surface melt is calculated using an enhanced temperature index model (Hock, 1999) and parameters for Austfonna derived by Schuler et al. (2007). Melt models use daily temperature data (either measured in-situ or from climate reanalysis products), together with calculated solar radiation receipts, to calculate melt. The ‘degree-day’ parameters relating temperature and solar radiation receipts to melting differ between ice and snow surfaces, to account for the lower albedo of ice. The model needs an initial snow cover at the start of the melt season; this is progressively removed by melt calculated using the degree-day factor for snow until glacier ice is exposed, at which point the model begins to use the factor for ice. Here, we use ERA-Interim climate reanalysis products (Dee et al., 2011) for temperature,

bias-corrected for Austfonna using data from T. Schuler (unpublished data), and snow-depth calculated using the relationships developed by Taurisano et al. (2007). Output of the melt model consists of daily melt totals in each cell of the ice-cap DEM. Refreezing of surface melt in the snowpack is important on high-latitude ice masses, and can delay (or even prevent) entry of water into the subglacial drainage system. Although complex multi-layer models have been developed to account for this process (e.g. Rye et al., 2012), given the basin-scale focus of this model we follow Schuler et al. (2007) and assume that water will penetrate through the snowpack to the glacier surface once the cumulative amount of melt exceeds 0.6 times the local snow depth. Once water has reached the ice surface, it is passed to the subglacial hydrological model.

Predicting meltwater drainage patterns beneath Austfonna

Our subglacial water-routing model utilises calculations of time-dependent meltwater flux through Austfonna (Arnold, 2010). The model calculates upstream area values across a DEM of the ice-cap bed, and allows ponding of water in depressions. Water held in depressions can spill downstream, preserving flow continuity (Arnold, 2010). The model utilised DEMs of the ice-surface elevation and ice thickness of Austfonna at 1 km resolution (Dowdeswell et al., 1986, 2008) to calculate the hydraulic potential surface, Φ, at the ice-cap bed (Shreve, 1972):

$$\Phi = \rho_w g z_b + K \rho_i g (z_s - z_b) \quad (1)$$

where ρ_w and ρ_i are bulk densities of water and ice, respectively, g is acceleration due to gravity, z_b is height of the ice-cap bed and z_s is ice-surface height. The potentiometric surface calculated by the model is regarded as the principal control on subglacial water flow (Shreve, 1972; Arnold et al., 1998).

Within the meltwater flow-routing model, the parameter K may be varied to reflect the subglacial water pressure and, therefore, the dominant configuration of the basal drainage system (Flowers and Clarke, 1999). Higher K values represent higher water pressures (up to a maximum of K=1, implying that water pressure equals ice overburden pressure), which are representative of relatively inefficient distributed subglacial drainage systems. Lower values (with K=0, implying water flow at atmospheric pressure) are characteristic of efficient, channelised drainage. A sensitivity test showing model predictions of drainage routing beneath Austfonna for four values of K between 0.25 and 1 is given in Figure 6A-D. Subglacial conduits are identified clearly with K = 0.25 or 0.5; when K > 0.5, the conduits

begin to merge along the margin of Austfonna as the modelled basal hydrological system becomes more distributed. Given our satellite-derived observations of numerous discrete turbid plumes emerging at the tidewater terminus of Austfonna (Figs. 2-4), it appears that lower values of K are most suitable for application to the numerical model of Austfonna's drainage pattern.

A second set of sensitivity tests (Fig. 6E-H) compares predictions of subglacial drainage pattern for the same day in a "cold" year (2001) and a "warm" year (2002), and also varies the way surface meltwater is allowed to penetrate to the bed of Austfonna. Drainage-system development and meltwater delivery to the margin is responsive to the amount of surface meltwater available to reach the bed and develop the basal drainage system. In the colder early summer of 2001, the model predicts that the basal drainage system is slow to develop, whereas at the same date in 2002 the pattern of subglacial drainage is already relatively well established by mid-July, assuming in both cases that runoff from the snowpack to the bed only takes place when melt within the snowpack is greater than 0.6 times snow depth (E and F). Further tests show the drainage pattern when melt within the snowpack is released to descend into the basal water system at 0.3 times snow depth (Fig. 6G-H); in this case, the numerical model predicts a better-developed basal system with a greater number of meltwater channels. Thus, a channelised basal drainage system is predicted to be most developed as water input from the ice surface increases and for lower values of K; that is at lower water pressures within the basal water system. However, it should be noted that changes in basal drainage network complexity and the number of marginal channels are relatively insensitive to changing water volumes (Fig. 6); whereas meltwater discharge rises linearly with increased surface meltwater availability to the basal system, the model-predicted increase in the number of basal channels is slow.

Comparing subglacial water routing predictions and observed turbid-plume locations

The drainage pattern beneath Austfonna predicted by the water-routing model for particular days has reasonable agreement with the mapped locations of meltwater plumes (Figs. 7, 8). The model predicts between 57% and 67% of plumes observed on satellite images, with the largest and most frequently occurring plumes (e.g. plumes 1, 5, 17, 34) very clearly predicted.

Plumes observed on satellite imagery but not predicted by the model are probably missing because of model resolution (1 km x 1 km grid-size). This is because plumes that are not spaced more than two pixels apart are not resolved by the model output; even plumes around

1 km apart would merge into a continuous "line" of output along the marine margin of Austfonna and would be difficult to distinguish. This is exemplified where there are many observed meltwater plumes per unit distance along the margin of Austfonna (i.e. along basins 6-9).

The water-routing model does not have the ability to change the locations of meltwater conduits over time because conduit position is constrained by the subglacial DEM and ice-thickness inputs to the model. This is acceptable, given that ice-cap surface and bed topography change only slowly through time, remaining effectively fixed over the decadal time-scale modelled here. The implication is that, whilst meltwater discharge may vary, the numerical model suggests that conduit locations along the ice front are likely to be stable on timescales of years to decades.

MODELLING MELTWATER PLUMES AND GLACIMARINE SEDIMENTATION RATES

Turbid meltwater plume model and input data

A turbid meltwater plume model, *SedPlume*, was developed to simulate sediment transport and deposition from glacial meltwater plumes as they enter the ocean at the base of tidewater glacier ice cliffs (Mugford and Dowdeswell, 2011). The conservation equations for flux of volume, momentum, buoyancy and sediment are solved following the formulation of Jirka (2004), but in two dimensions. To solve the equations for a turbulent, entraining plume injected at an angle into stationary, stably stratified ambient fluid, the equations are formulated so that the ordinary differential equations are solved along the plume path and the integrals are solved across the Gaussian cross-section of the plume.

Sediment deposition is included following Lane-Serff and Moran (2005), with sedimentation occurring when the radial component of sediment-fall velocity (according to Stokes' Law) exceeds entrainment velocity. Mean entrainment velocity is taken to be directly proportional to mean plume centre-line velocity, where the proportionality constant, determined by experimental measurements, equals 0.1 (Morton, 1959). Flocculation of silt and clay particles in saline water is included by using empirical measurements of particle settling velocities in fjords to adjust the settling velocity of fine-grained sediments. At the sea surface, the plume is assumed to behave as a radially spreading surface-gravity current, for which there are analytical solutions for sediment deposition rate (Sparks et al., 1991; Bonnecaze et al., 1995).

Sensitivity tests with the *SedPlume* model (Fig. 9), show how the rate of sedimentation varies with distance offshore from a conduit mouth at the base of a tidewater glacier for a number of values for meltwater discharge (Fig. 9A), conduit radius (Fig. 9B), initial suspended-sediment concentration (Fig. 9C), and the proportion of sand-sized debris (Fig. 9D). As parameter values rise, so too do rates of ice-proximal deposition, fan length and volume (Fig. 9). Model-predicted sedimentation rates within about 100 m of a melt-stream portal vary in an envelope from about 0.03 cm d^{-1} to 0.6 cm d^{-1} for a range of examples (Fig. 9).

Predicting patterns and volumes of sediment delivery to ice-proximal fans

The *SedPlume* model can be run for specified values of particle size (sand-silt-clay fraction), meltwater discharge, conduit radius and initial suspended-sediment concentration in the plume. Taking field observations offshore of Austfonna, where available, we used particle-size data from sediment cores in ice-proximal locations in Hartogbukta (Figs. 1B, 10) and plume-turbidity data from water samples collected offshore of Basin 3 by Pfirman and Solheim (1989). Using an initial suspended-sediment concentration of 50 mg l^{-1}, fairly typical for Svalbard melt streams, the model predicts the rate of sediment rain-out with distance from a subglacial portal for a time-series of meltwater discharge derived from the ice-cap surface melt model described earlier. Results are shown for summer 2006, where the discharge hydrograph in Figure 11A from Basin 4 of Austfonna delivers meltwater to a conduit margin through the season. Sedimentation by rain-out declines exponentially with increasing distance offshore (Fig. 11B). Total sedimentation during summer 2006 is predicted to be about 1.6 cm within 100 m of the conduit mouth, declining to only 0.5 and 0.15 cm at distances of 500 m and 1,000 m, respectively (Fig. 11B). The total volume of sediment delivered to the ice-proximal marine setting during this single melt season is about 6.1 x 10^{-6} km^3, building a fan of predicted radius about a kilometre (Fig. 11B, C). Using the discharge hydrograph (Fig. 11A), the model can also predict variations in sedimentation over the melt season (Fig. 11B). July has the greatest sediment delivery, linked to peak surface melting and discharge from the ice cap. Varying any of the key parameters driving the model will alter the dimensions of the fan, affecting both its radius and thickness (Fig. 9).

Using parameter values derived from field observations of ice-cap mass balance, water turbidity and particle-size distributions, fan thickness is likely to build at rates of centimetres per year, and volume at about 6 x 10^{-6} km^3 yr^{-1}, in the regional climatic and glacier mass-balance setting of eastern Svalbard today, assuming a suspended-sediment concentration of

50 mg l^{-1} (Fig. 11). This rate of sediment accumulation is of a similar order to observations within a few hundred metres of the tidewater glacier margins in Spitsbergen fjords, where deposition rates of 7 cm yr^{-1} have been recorded (Elverhøi et al., 1983; Görlich et al., 1987). Thus, for a period of, say, 10 years of stability in conduit-mouth location, a fan of up to a few tens of centimetres in thickness and a volume of 60 x 10^{-6} km^3 may be produced.

In areas of higher mass-throughput where tidewater glaciers occur, for example at fjord heads in south-east Alaska and southern Chile (e.g. Powell and Molnia, 1989; Powell, 1990; Dowdeswell and Vasquez, 2013), and precipitation is several metres per year, total melt-season discharge may be one to two orders of magnitude greater than in eastern Svalbard, where precipitation is only a few hundred millimetres per year (Hagen et al., 1993). Increasing discharge by one and two orders of magnitude, to simulate these glacimarine settings using *SedPlume*, fan volume over a ten-year period is predicted to increase to between 6 x 10^{-4} km^3 and 1.6 x 10^{-3} km^3 with a thickness of between 40 and 50 cm within 200 m of the conduit mouth (Fig. 11D). In addition, the radius of the ice-proximal fan will also increase, to extend several kilometres from the melt-stream portal (Fig. 11D).

The rate of build-up of ice-proximal sediment, often in the form of a fan extending from the grounding-line, has been observed within a few kilometres of tidewater glacier margins in Alaskan fjords (e.g. Cowan and Powell, 1990; Powell, 1990). Seramur et al. (1997) reported that an ice-proximal fan of about 0.8 km^3 and radius about 4 km formed over a 20 year-period of terminus stability at the margin of Muir Glacier in Alaska. This is two orders of magnitude or more greater than the model predictions using discharge rates elevated above those for Austfonna (Fig. 11D), implying that the initial concentration of sediment in plumes from Alaskan tidewater glaciers may be considerably greater than the 50 mg l^{-1} assumed for Svalbard in Figure 11A. This is consistent with observations of suspended-sediment concentrations of several hundred milligrams per litre in Alaskan proglacial streams (Hoskin and Burrell, 1972; Cowan and Powell, 1990).

ICE-PROXIMAL FANS AT TIDEWATER ICE MARGINS

Modern ice-proximal fans offshore of Austfonna

Offshore of Austfonna, about 200 km^2 of swath-bathymetric and sub-bottom profiler data (Fig. 1B) shows the presence of a fan associated with a large moraine about 20 m high within 10 km of the present ice front (Fig. 12). The fan is almost a kilometre long and may be up to about 20 m thick at its ice-proximal maximum, although a basal reflection cannot be traced clearly other than beneath the distal toe of the fan (Fig. 12C, D). We interpret this feature as

an ice-proximal fan produced at a former ice-marginal position of Austfonna in Hartogbukta. Increased penetration of our sub-bottom profiler at the distal end of the depocentre suggests fining towards its toe, which would be expected in such a system (Powell, 1990; Mugford and Dowdeswell, 2011). Inshore of the fan and moraine ridge is a series of smaller recessional moraines together with several polygonal and occasionally streamlined sediment lobes (Robinson and Dowdeswell, 2011). This area of Hartogbukta, adjacent to Basins 4 and 5, has experienced the almost continuous presence of summer meltwater plumes since at least 1976 (Fig. 4). Furthermore, at decadal timescales, the ice front has been retreating for at least the past 40 years (Fig. 5), with minor readvances of parts of Basins 3 and 4 during the early 1990s and since 2012 (Dowdeswell et al., 1999; McMillan et al., Submitted). However, there is a lack of clearly identifiable ice-proximal fans over much of the sea-floor of Hartogbukta, inshore of the large moraine ridge and associated fan (Fig. 12). These findings suggest that the formation of well-defined ice-proximal fans requires not only sediment delivery from subglacial streams to portals at the terminus, but also that the terminus remains stable over periods of years to decades to allow significant depocentres to form.

There are several relatively small polygonal sediment lobes between the prominent moraine ridge and fan complex and the limit of our geophysical data coverage close to Austfonna (Fig. 12A, B). These features suggest that, although deposition is taking place each summer at melt-stream mouths, the ice front remains in a stable position for insufficient time for the clearly identifiable geometry of 'classical' ice-proximal fans (sometimes referred to as 'grounding-line fans' – Powell, 1990; Seramur et al., 1997) to have developed close to tidewater glacier grounding-lines (Fig. 13A). Additional support for this interpretation comes from the observation that some small depositional lobes are organised sub-parallel to the direction of former ice flow and, therefore, to the likely orientation of subglacial channels orthogonal to the retreating ice margin (Figs. 12A, B, 13F).

Although diagrams of 'classical' ice-proximal fans have appeared in several review papers and textbooks (e.g. Powell, 1990; Powell and Domack, 1995; Benn and Evans, 2010), primary evidence in the form of similar well-defined fan-shaped submarine landforms imaged in swath-bathymetric data from modern fjord systems is sparse. This is not to say that the processes leading to ice-proximal fan formation have been incorrectly specified, but that ice-margin terminus retreat may preclude their full development. Furthermore, it may sometimes be easier to identify ice-proximal fans in high-resolution shallow-acoustic records than in the plan-form view offered by swath bathymetry (e.g. Seramur et al., 1997).

A schematic model for ice-proximal fans

We present three schematic models, and associated swath-bathymetric examples, of ice-proximal deposits (IPDs) that represent different periods of stability of marine-terminating ice margins (Fig. 13). First, where an ice margin remains in a stable position for one to several decades, sedimentation from a meltwater plume builds up to form a clearly defined ice-proximal fan (Fig. 13A). We might call this a 'classical' ice-proximal fan, similar to the early drawings of Powell (1990). Swath-bathymetric data from adjacent to the tidewater margin of Kronebreen, in Kongsfjorden, northwest Spitsbergen, appear to represent depocentres of this type (Fig. 13B), as documented by Trusel et al. (2010) and Kehrl et al. (2011). A second schematic model represents a quasi-stable ice margin, in which a glacier readvance (which may take place during winter or over a few years) pushes or thrusts up ice-proximal deposits, including fan material, to form a morainal ridge or bank complex (MBC in Fig. 13C). In this case, at least part of the fan morphology and stratigraphy may be preserved. Potentially, instability caused by oversteepening may lead to slope failure and the deposition of debrites, similar to debris flows and sediment lobes observed distal to some Svalbard submarine moraine ridges (Ottesen and Dowdeswell, 2006). This is our interpretation of the large moraine ridge in Hartogbukta, where moraine ridge and fan components are both present (Fig. 12). In a third case, a retreating ice margin with only episodic and brief still-stands over decades allows small accumulations of ice-proximal deposits close to the grounding-line to build up at meltwater plume locations (Fig. 13E), but a fully formed and clearly identifiable 'classical' concentric fan does not develop. These small lobe-like ice-proximal deposits are imaged in Hartogbukta within about 3 km of the present ice margin (Fig. 13F). The lobe-like submarine landforms occur in conjunction with small ridges, just a metre or a few metres in height, which were reported offshore of Austfonna by Solheim and Pfirman (1985) and Solheim (1991) and interpreted as recessional moraines indicating brief still-stands or minor winter readvances of a generally retreating ice margin (Fig. 13F). Similar annual-retreat ridges have been observed in Svalbard fjords by Ottesen and Dowdeswell (2006). This three-part schematic model of grounding-line and immediately ice-proximal process and form thus takes account of stability, or lack of it, at ice-mass termini, which restricts the time available to build an ice-proximal fan in many modern situations where tidewater glaciers and ice caps are in overall retreat (IPCC, 2013).

Some large ice-proximal sub-aqueous fans (>5 km^3 in volume) recorded at the margins of Quaternary and ancient tidewater glaciers, and those terminating in lakes, may result from short-lived outburst floods or jokulaups; high discharge rates have been interpreted from

transcritical to supercritical bedforms observed within the sediments (Russell and Arnott, 2003; Winseman et al., 2009; Hirst, 2012). These high-magnitude events can deliver vast quantities of meltwater from the rapid drainage of subglacial or ice-dammed lakes over hours to days. In these cases, the location of the glacier terminus remains essentially unchanged for the duration of the event. Thus, such high-magnitude events may build ice-proximal fans, tens of metres in thickness and several kilometres in radius, whereas lower magnitude discharge over periods of years may fail to build clearly identifiable depocentres because the ice margin is mobile at these longer timescales (Fig. 13C, E).

Ancient ice-proximal fans in the Late Ordovician glacial rocks of northern Africa

During the Lower Palaeozoic, the supercontinent of Gondwana was located around the South Pole (e.g. Scotese et al., 1999). Sedimentation was dominated by fluvial and shallow-marine settings during much of this time, but a short-lived (~1-2 My) glacial episode is recorded in the latest Ordovician (e.g. Hambrey and Harland, 1981; Beuf et al., 1971; Vaslet, 1990; Moreau et al., 2005; Le Heron and Craig, 2008). The Late Ordovician ice sheet covered a large part of North Africa and Arabia (McClure, 1978; Vaslet, 1990; Le Heron and Craig, 2008). Algeria and Libya are interpreted to have been ice-covered during the Late Ordovician glacial maximum (Le Heron and Craig, 2008). During this time, and the initial deglaciation, glacial valleys were eroded into the pre-glacial semi-consolidated, often sandy substrate (Hirst et al., 2002; Moreau et al. 2005; Le Heron and Craig, 2008; Hirst, 2012). The valleys were then largely filled during ice-sheet retreat by a complex assemblage of glacigenic, glacimarine and related sediments (e.g. Hirst et al., 2002; Hirst, 2012; Lang et al., 2012).

Four main sedimentary facies groups have been identified in the Illizi Basin of Algeria (Hirst et al., 2002; Hirst, 2012): fine- to medium-grained sandstones with tractional bedforms (Fig. 14B); massive to low-angle cross-bedded fine-grained sandstones (Fig. 14B); heterolithics comprising very fine-grained sandstones and laminated mudstones with rare granules (Fig. 14B); and poorly sorted argillaceous sandstones with granules and deformed fabrics (Fig. 14D). Sandstones with tractional bedforms occur mainly in the lower parts of glacial valley fills. They have limited lateral extent at outcrop (typically <200 m wide and <10 m thick) and are interpreted as subglacial channel-fills (Hirst et al., 2002; Dixon et al., 2008); similar thicknesses are noted in wells and subsurface widths are predicted to be similarly limited. These ice-proximal fans and associated deposits are referred to in detail in Figure 14 (A, B). Massive to low-angle cross-bedded sandstones are more common in the

uppermost valley fills and in strata that overtop the valleys to form a regionally extensive blanket. The sandstones occur mainly as laterally extensive (10s of kilometres) amalgamated sheets and channels, cumulatively several tens of metres thick. They are interpreted as proglacial high-density turbidites deposited by occasional high-magnitude glacial meltwater events, possibly related to periodic catastrophic draining of subglacial lakes (Hirst, 2012). The heterolithic to mudstone facies are interpreted as ice-distal deposits comprising the distal expression of meltwater turbidites and hemipelagic sedimentation with rain-out material from icebergs and turbid meltwater plumes between the high magnitude events (Fig. 14A, B). Finally, poorly sorted argillaceous sandstones with granules and deformed fabrics are interpreted as debris-flow deposits, shed from unstable sediments accumulated in front of tidewater-glacier termini and subaqueous valley walls. These deposits, a result of probable slope failures on morainal banks that produce debris flows, are shown in Figure 14 (C, D).

The proglacial turbidite sandstones form a major hydrocarbon reservoir target. Their extensive development in the uppermost Late Ordovician glacial stratigraphy is probably related to stillstands during the final, relatively rapid retreat of the marine-terminating ice sheet. The precursor glacial-valley network occurs as tens of kilometres-long and approximately S-N to SE-NW orientated incisions with abrupt beginnings and ends. Mega-regional mapping of the glacial sediment isopach reveals thicks orientated perpendicular to the ends of these valley trends (Le Heron and Craig, 2008). These large-scale patterns are consistent with phased or episodic ice-sheet retreat in which sedimentary depocentres in front of ice-sheet grounding lines built up during stillstands (Le Heron and Craig, 2008). Ice-proximal fans would be expected to form in front of these ancient ice-sheet grounding lines, especially where meltwater was emerging from subglacial channels at point sources (e.g. Lønne et al., 2001; Powell and Cooper, 2002), providing a model to predict reservoir presence in the subsurface.

We present schematic models of the sediments and sedimentary processes associated with tidewater glacier margins in what were apparently relatively mild palaeo-glacial conditions at the retreating margins of a Late Ordovician North African ice sheet where meltwater was abundant (Fig. 14A, C). The models are based on outcrop observations in Algeria and Libya, supported by photographs of cores through these sediments (Fig. 14B, D). They complement the three schematic models (Fig. 13A, C. E), derived mainly from geophysical observations of the modern sea-floor landforms in Svalbard (Fig. 13B, D, F), in that they are produced largely from the examination of ancient glacimarine sediments exposed above sea-level in outcrop.

In the schematic model of Late Ordovician ice-proximal fans and related sediments (Fig. 14A), relatively coarse-grained, cross-bedded sandstones are interpreted to represent former subglacial meltwater channels. Further moderately well-sorted and cross-bedded sandstones are interpreted to make up the most ice-proximal part of a fan system; these are tractional sediments deposited close to subglacial stream portals as meltwater jets expanded rapidly and decelerated upon exiting confining channels. These most ice-proximal fan sediments grade into well-sorted to weakly laminated sandstone and, more ice-distally, into well-sorted muddy sandstone (Fig. 14A, B), representing progressively more distal turbidites linked to occasional underflows of very dense and turbid meltwater. Sedimentation of this distally fining sequence is inferred to have taken place within a few kilometres of the ice margin and was probably also contributed to by rain-out of fine sands and silts from turbid meltwater plumes. In the subsurface of the Illizi Basin, the sand prone component of the larger of these subaqueous outwash events can be tracked for 10 to 15 km in radius; in the proximal areas, a single event may have deposited 2 to 3 m of sandstone (Hirst, 2012) although, typically, the fans were smaller and thinner than this. In ice-distal settings, tens of kilometres away from the meltwater sources of suspended sediments, well-sorted heterolithic sandstones and, eventually, laminated and largely hemipelagic mudstones are found (Fig. 14A, B); these formed as alternations of distal turbidites and rain-out of fine-grained material from meltwater plumes. Rafting from icebergs is likely to have provided some outsized clasts or dropstones even within these ice-distal environments.

A second schematic model is focused on areas of former ice-fronts that were remote from subglacial channel mouths (Fig. 14C, D). Here, sedimentation was dominated by slope failure on the ice-distal sides of morainal bank complexes (Fig. 13B). This led to debris flows and the deposition of poorly sorted debrites, together with highly deformed heterolithics representing slumps (Fig. 14C, D). In more distal settings, sedimentation was likely to be similar to distal meltwater-plume influenced areas, with sedimentation rates perhaps somewhat slower.

There are additional specific aspects of the regional geology which may have influenced the characteristics of sedimentation in North Africa. First, because the semi-consolidated rocks underlying the Late Ordovician glacial sequence in much of Algeria and Libya include significant intervals of well-sorted fluvial and shallow-marine sandstones, sand-grade sediment was widely available and easily removed when glacial and glacifluvial erosion occurred. In glacial environments, ancient and modern, where a sandy substrate is not present, the mainly sandy sediments illustrated in Figure 14B may be replaced predominantly

by fine sand, silt and clay where finer-grained sediments are being eroded by overlying ice (except where traction load is deposited close to a former ice margin). Secondly, the localised development of resistant basement highs potentially stabilised the ice front for extended periods, allowing the development of larger fans (Hirst, 2012). Key challenges in better understanding the Late Ordovician North African glacigenic and related sedimentary system are in determining the likely meltwater and sediment fluxes to the ice front. Simple modelling of the above using sensible boundary conditions (Le Heron and Dowdeswell, 2009) will provide constraints on meltwater-plume locations and fluxes over time and, hence, test and refine predictions of outwash fan sandstone distribution in the subsurface.

Ice-proximal fans as indicators of past glacimarine environments

Where ice-proximal fans are found in the glacier-influenced marine record, the implication is that abundant meltwater was available to form a network of subglacial drainage channels that delivered sediment to tidewater-glacier margins at point sources. Much of this meltwater is derived initially from ice-surface melting during summer. Thus, the ice-proximal fans reported from, for example, the Late Ordovician rocks of Northern Africa and the Permian Pagoda Formation in Antarctica, imply that the environmental setting at these ancient marine ice-sheet margins was relatively mild with abundant meltwater (Hirst, 2012; Koch and Isbell, 2013); that is, conditions similar to the glaciological, climatic and oceanographic settings found in south-east Alaska, southern Chile or Svalbard today (e.g. Elverhøi et al., 1983; Powell and Molnia, 1989; Dowdeswell and Vasquez, 2013). These modern locations have relatively high mass-turnover on the ice surface, with high to intermediate levels of snow precipitation and offshore water temperatures of several degrees centigrade, where strong surface melting is the major contributor to mass loss. Indeed, the Late Ordovician glacigenic rocks of northern Africa also contain evidence of tunnel valleys (e.g. Ghienne and Deynoux, 1998; Hirst et al., 2002; Le Heron et al., 2004), formed by meltwater flow in large subglacial channels (Ó Cofaigh, 1996); similar features are observed widely in the relatively mild Late Quaternary full-glacial environment of the North Sea (e.g. Stewart and Lonergan, 2011).

By contrast, in high-polar locations, where precipitation is restricted to a few centimetres per year and air and water temperatures are very low (e.g. water <0 to -1.5°C), mass is lost at ice-sheet margins mainly by the production of icebergs and basal melting of floating ice shelves (Rignot et al., 2013), and surface melting is either low or almost non-existent. These conditions are present today in much of East Antarctica and in northern Ellesmere Island in the Canadian high Arctic and northernmost Greenland. In these more severe climatic and

oceanographic conditions, offshore sedimentation takes place at very low rates and is generally derived from diamictic debris released from slowly melting icebergs (e.g Dowdeswell et al., 1994). In the coldest modern environments of East Antarctica, for example the George V Land coast, water temperatures of <-1°C mean that even large icebergs may transverse the inner shelf without significant melting and debris release, and sedimentation is predominantly through the rain-out of biogenic micro-organisms to produce a slowly accumulating ooze with limited iceberg-rafted debris (e.g. Domack, 1988).

INITIAL NUMERICAL-MODEL PREDICTIONS OF BROAD-SCALE WATER FLOW FROM A LATE ORDOVICIAN ICE SHEET

In ancient, pre-Quaternary glacial environments, where even the general glaciological and topographic setting may be poorly known, a numerical-modelling approach can be adopted to allow prediction of meltwater discharge and the broad pattern of subglacial drainage. Such modelling has potential applicability to palaeo-ice sheets, where assumptions about past climatic regime are required, together with either geological information or assumptions about the overall configuration of the former ice sheet. Examples of simple information on past climate and ice-sheet geometry and organisation for the Late Ordovician glaciation of Northern Africa include work by Le Heron and Craig (2008) and Le Heron and Dowdeswell (2009). This information is used here in simple modelling of meltwater production and water discharge beneath the North African Ice Sheet about 445 M yr ago.

We use a one-dimensional long-profile numerical ice-sheet model (a Matlab adaptation of the model of Pattyn, 2005), and apply three different climate and glacier mass-balance relationships; ‘warm’ where sea-level summer temperature is 4°C, and two ‘cool’ scenarios where summer temperatures are -1°C and -10°C (Le Heron and Dowdeswell, 2009). This initial modelling was undertaken to investigate the effects on water flow of the presence or otherwise of fast-flowing ice streams within the Late Ordovician ice sheet, a situation inferred from geological evidence in the reconstruction of Le Heron and Craig (2008). For each palaeoclimatic scenario, the model was run until an equilibrium ice sheet was formed, whose shape was a direct response to an imposed climate and calculated mass balance. The basal-sliding velocity and total summer meltwater discharge are shown in Figures 15A and B. Note that ice velocity and meltwater discharge are considerably higher for the ‘warm’ scenario and meltwater production also takes place further into the interior of the ice sheet (Fig. 15B).

Given that here we are concerned with the production and routing of meltwater to the former ice-sheet margin, we focus on the pattern of water discharge for the Late Ordovician ice-sheet marine terminus with a series of ice streams, each set about 500 km or so apart, located between slower-flowing ice. This is the situation mapped by Le Heron and Craig (2008), who suggested the presence of seven ice streams, spaced along the 4,000 km-long northern margin of the Late Ordovician North African ice sheet. The principal finding of this initial modelling is that water discharge is highest at the lateral margins of the seaward terminus of each of several modelled ice streams (Fig. 15C). This is because thicker ice, beneath the centre of each ice stream at its distal end, forces subglacial water-flow to the ice-stream lateral margin down a water-pressure gradient. Note also that water discharge is lower along the interior ice-stream margins of the ice sheet (Fig. 15C); here, the thicker ice within the slower moving areas adjacent to the ice streams forces water under the ice streams. Finally, this broad-scale modelling also suggests, through a stability analysis of subglacial channels (Arnold and Sharp, 2002), that the basal tunnels are potentially stable near the ice sheet margin in inter-ice stream areas (due to high water discharges favouring wall melting over tunnel closure by ice deformation), but are unstable beneath the fast-flowing palaeo-ice streams themselves. This is because faster ice flow increases tunnel closure rates. At the distal lateral margins of the ice streams, however, the combination of lower velocity but higher water discharge (due to water flow towards the lateral margins of the ice streams as discussed above) allows stable tunnels to exist a little way into the ice sheet interior (Fig. 15D).

The implications for water flow are that, except close to their lateral margins, palaeo-ice streams are unlikely to be drained by channelised water flow, and that meltwater discharge is likely to be greatest at ice-stream margins. This suggestion matches well with swath-bathymetric images of Quaternary ice-stream beds, such as those from cross-shelf troughs around Greenland and Antarctica. Here, sedimentary landforms produced beneath Quaternary ice streams, and preserved on the sea-floor after rapid deglaciation, show no evidence of channelised meltwater flow (e.g. Ó Cofaigh et al., 2002; Livingstone et al., 2012; Dowdeswell et al., 2014).

CONCLUSIONS

Turbid meltwater plumes and ice-proximal fans occur where subglacial streams reach the grounded marine margins of modern and ancient tidewater glaciers. The spacing and temporal stability of these subglacial channels is, however, poorly understood. This has

significant implications for understanding the geometry and distribution of modern, Quaternary and more ancient ice-proximal fans that can form important aquifers and hydrocarbon reservoirs. Remote-sensing and numerical-modelling techniques have been applied to a Svalbard ice cap, Austfonna, and its 200 km-long marine margin (Fig. 1), in order to quantify turbid meltwater-plume distribution and to predict the temporal stability of the basal drainage system. These investigations were combined with marine-geophysical data acquired within a few kilometres of the modern ice front of Austfonna to refine existing depositional models for ice-proximal fan sedimentation.

Modern meltwater plumes of suspended sediment, derived from the basal drainage system of Austfonna, are spaced on average about 3 km apart and their distribution along the ice front is consistent over several decades (Figs. 3, 4). Numerical modelling also predicts the drainage pattern and time-dependent meltwater discharge beneath the ice cap, with modelled water-routing patterns in reasonably good agreement with satellite-mapped plume locations (Figs. 7, 8). However, glacier-terminus retreat of several kilometres over the past 40 years east of Austfonna (Fig. 5) has limited the build-up of significant ice-proximal fans because the focus of sediment delivery is migrating back with the retreating ice-cap margin. A single fan and associated moraine ridge is noted from marine-geophysical surveys of a 200 km^2 area offshore of the ice cap (Fig. 12). Closer to the ice front there are smaller recessional moraines and polygonal sediment lobes, representing short-term locations of the ice front, but no identifiable fans (Fig. 12). This suggests that fan formation requires not only sediment delivery from meltwater streams, but also a stable tidewater glacier terminus over timescales of years to decades in order to enable a significant depocentre to form. Numerical modelling can also be used to simulate sediment transport and deposition from glacial meltwater plumes. Using values from eastern Svalbard, model-predicted sedimentation rates close to melt-stream portals were between 0.03 cm d^{-1} and 0.6 cm d^{-1} (Fig. 9) with total predicted sedimentation of about 1.6 cm yr^{-1} adjacent to a conduit mouth (Fig. 11). In areas of higher glacier mass-throughput, such as the fjords of Alaska and Patagonia, total melt-season discharge and sediment delivery to the ice-proximal environment may be one to two orders of magnitude greater than in Svalbard, resulting in more rapid fan development (Fig. 11D).

Several schematic models of ice-proximal deposits are therefore required in order to represent variations in glacier-terminus stability and associated glacimarine sedimentation (Fig. 13): (i) a stable terminus where meltwater deposition produces an ice-proximal fan; (ii) a quasi-stable terminus, where glacier readvance pushes or thrusts up ice-proximal deposits into a morainal bank, modifying any fan that has developed; and (iii) a retreating terminus,

with brief still-stands, allowing only small sediment lobes rather than a well-defined fan to build up at melt-stream portals.

These modern investigations are complemented with outcrop and subsurface observations and numerical modelling of an ancient, Ordovician glacial system. Two further schematic models of ice-proximal glacimarine sedimentation, based on cores and outcrop observations in Algeria and Libya, illustrate deposition at the margin of a Late Ordovician North African ice sheet, where meltwater was apparently abundant (Fig. 14). Thick turbidite successions and large fans (>5 km^3) recorded at the marine margins of Late Ordovician ice sheets suggest either short-lived high-magnitude outburst floods or sustained high discharge events during which the ice margin is stable, consistent with a relatively mild palaeo-glacial setting in which meltwater delivery of sediments in the dominant process.

In ancient, pre-Quaternary glacial environments, where even the general glaciological and topographic setting is poorly known, numerical modelling can also be used to predict the broad pattern of subglacial drainage (Fig. 15). Water discharge is highest at the lateral margins of the marine termini of several ice streams within a modelled Late Ordovician North African ice sheet (Fig. 15C). Thicker ice beneath the centre of each ice stream forces subglacial water-flow to the ice-stream lateral margins down a water-pressure gradient, implying that, except close to lateral margins, palaeo-ice streams are unlikely to be drained by channelized water flow.

ACKNOWLEDGEMENTS

We thank BP Algeria for sponsorship, Ed Jones and Liz Jolley of BP for supporting the project, and Toby Benham for assistance with satellite data analysis. Permission for presenting the bathymetric data was granted by Norwegian Hydrographic Service (permission nr. 14/G754).

REFERENCES

Arnold, N. (2010) A new approach for dealing with depressions in digital elevation models when calculating flow accumulation values. *Progress in Physical Geography*, **34**, 781-809.

Arnold, N.S. and Sharp, M.J. (2002) Flow variability in the Scandinavian Ice Sheet: modelling the coupling between ice sheet flow and hydrology. *Quaternary Science Reviews*, **21** 485-502.

Arnold, N., Richards, K., Willis, I. and Sharp, M. (1998) Initial results from a distributed, physically based model of glacier hydrology. *Hydrological Processes*, **12**, 191-219.

Barry, R.G. (2006) The status of research on glaciers and global glacier recession: a review. *Progress in Physical Geography*, **30**, 285-306.

Benn, D.I. and Evans, D.J.A. (2010) *Glaciers and Glaciation* (2nd Edition). London, Arnold.

Benn, D.I., Warren, C.R. and Mottram, R.H. (2007) Calving processes and the dynamics of calving glaciers. *Earth-Science Reviews*, **82**, 143-179.

Beuf, S., Biju-Duval, B., de Charpal, O., Rognon, P., Gariel, O. & Bennacef, A. (1971) Les Grès du Paleáozoïque Inférieur au Sahara. Editions Technip, Paris.

Błaszczyk, M., Jania, J.A. and Kolondra, L. (2013) Fluctuations of tidewater glaciers in Hornsund Fjord (Southern Svalbard) since the beginning of the 20th century. *Polish Polar Research*, **34**, 327-352.

Bonnecaze, R.T., Hallworth, M.A., Huppert, H.E. and Lister, J.R. (1995) Axisymmetrical particle-driven gravity currents. *Journal of Fluid Mechanics*, **294**, 93–121.

Chu, V.W., Smith, L.C., Rennermalm, A.K., Forster, R.R. and Box, J.E. (2012) Hydrologic controls on coastal suspended sediment plumes around the Greenland Ice Sheet. *The Cryosphere*, **6**, 1-19.

Cook, A.J., Fox, A.J., Vaughan, D.G. and Ferrigno, J.G. (2005) Retreating glacier fronts on the Antarctic Peninsula over the past half-century. *Science*, **308**, 541-544.

Cowan, E.A. and Powell, R.D. (1990) Suspended sediment transport and deposition of cyclically interlaminated sediment in a temperate glacial fjord, Alaska, USA. *In* Dowdeswell, J.A. and Scourse, J.D., (Eds), Glacimarine Environments: Processes and Sediments. *Geological Society, London, Special Publication*, **53**, 75-89.

Dee, D.P., and 35 others (2011). The ERA-Interim reanalysis: configuration and performance of the data assimilation system. *Quarterly Journal of the Royal Meteorological Society*, **137**, 553–597.

Dixon, R.J., Patton, T.L. & Hirst, J.P.P. (2008) Giant sandwaves from the Late Ordovician of the Tassili N'Ager, Algeria. Extended Abstract, Marine and River Dune Dynamics, 1–3 April 2008, Leeds, UK.

Domack, E.W. (1988) Biogenic facies in the Antarctic glacimarine environment: basis for a polar glacimarine summary. *Palaeogeography, Palaeoclimatology, Palaeoecology*, **63**, 357-372.

Dowdeswell, J.A. (1986) Drainage-basin characteristics of Nordaustlandet ice caps, Svalbard. *Journal of Glaciology*, **32**, 31-38.

Dowdeswell, J.A. (1989) On the nature of Svalbard icebergs. *Journal of Glaciology*, **35**, 224-234.

Dowdeswell, J.A. and Vasquez, M. (2013) Submarine landforms in the fjords of southern Chile: implications for glacimarine processes and sedimentation in a mild glacier-influenced environment. *Quaternary Science Reviews*, **64**, 1-19.

Dowdeswell, J.A., Drewry, D.J., Cooper, A.P.R, Gorman, M.R., Liestøl, O. and Orheim, O. (1986) Digital mapping of the Nordaustlandet ice caps from airborne geophysical investigations. *Annals of Glaciology*, **8**, 51-58.

Dowdeswell, J.A., Whittington, R.J. and Marienfeld, P. (1994) The origin of massive diamicton facies by iceberg rafting and scouring, Scoresby Sund, East Greenland. *Sedimentology*, **41**, 21-35.

Dowdeswell, J.A., Hagen, J.O., Björnsson, H., Glazovsky, A.F., Harrison, W.D., Holmlund, P., Jania, J., Koerner, R.M., Lefauconnier, B., Ommanney, C.S.L. and Thomas, R.H., 1997. The mass balance of circum-Arctic glaciers and recent climate change. *Quaternary Research*, 48, 1-14.

Dowdeswell, J.A., Unwin, B., Nuttall, A.-M. and Wingham, D.J. (1999) Velocity structure, flow instability and mass flux on a large Arctic ice cap from satellite radar interferometry. *Earth and Planetary Science Letters*, **167**, 131-140.

Dowdeswell, J.A., Benham, T.J., Strozzi, T. and Hagen, J.O. (2008) Iceberg calving flux and mass balance of the Austfonna ice cap on Nordaustlandet, Svalbard. *Journal of Geophysical Research*, **113**, doi:10.1029/ 2007JF000905.

Dowdeswell, J.A., Hogan, K.A., Ó Cofaigh, C., Fugelli, E.M.G., Evans, J. and Noormets, R. (2014) Late Quaternary ice flow in a West Greenland fjord and cross-shelf trough system: submarine landforms from Rink Isbrae to Uummannaq shelf and slope. *Quaternary Science Reviews*, **92**, 292-309.

Elverhøi, A., Lønne, Ø. and Seland, R. (1983) Gaciomarine sedimentation in a modern fjord environment, Spitsbergen. *Polar Research*, **1**, 127-149.

Flowers, G.E. and Clarke, G.K.C. (2002) A multicomponent coupled model of glacier hydrology. 1. Theory and synthetic examples. *Journal of* Geophysical Research, **107**, doi:10.1029/2001JB001122.

Ghienne, J.-F. and Deynoux, M. (1998) Large-scale channel fill structures in late Ordovician glacial deposits in Mauritania, western Sahara. *Sedimentary Geology*, **119**, 141-159.

Girard, F., Ghienne, J.F. and Rubino, J.-L. (2012) Channelized sandstone bodies ('cordons') in the Tassili N'Ajjer (Algeria & Libya): snapshots of a Late Ordovician proglacial outwash plain. In: Huuse, M., Redfern, J., Le Heron, D.P., Dixon, R.J., Moscariello, A. & Craig, J. (eds) Glaciogenic Reservoirs and Hydrocarbon Systems. Geological Society, London, Special Publications, **368**, 355-379.

Görlich, K., Weslawski, J.M. and Zajaczkowski, M. (1987) Suspension settling effect on macrobenthos biomass distribution in the Hornsund fjord, Spitsbergen. *Polar Research*, **5**, 175-192.

Hambrey, M.J. and Harland, W.B. (1981) Earth's Pre-Pleistocene Glacial Record. Cambridge University Press, Cambridge.

Hagen, J.O., Liestgl, O., Roland, E., and Jgrgensen, T. (1993) Glacier Atlas of Svalbard and Jan Mayen. *Norsk Polarinstitutt Meddelelser*, **129**, 141 pp.

Hagen, J.O., Melvold, K., Pinglot, F. and Dowdeswell, J.A. (2003) On the net mass balance of the glaciers and ice caps in Svalbard, Norwegian Arctic. *Arctic, Antarctic and Alpine Research*, **35**, 264-270.

Hirst, J.P.P., Benbakir, A., Payne, D.F. and Westlake, I.R. (2002) Tunnel valleys and density flow processes in the Upper Ordovician glacial succession, Illizi Basin, Algeria: influence on reservoir quality. *Journal of Petroleum Geology*, **25**, 297-324.

Hirst, J.P.P. (2012) Ordovician proglacial sediments in Algeria: insights into the controls on hydrocarbon reservoirs in the Ameneas field, Illizi Basin. *In* Huuse, M., Redfern, J., Le Heron, D.P., Dixon, R.J., Moscariello, A. and Craig, J., (Eds), Glaciogenic Reservoirs and Hydrocarbon Systems, *Geological Society, London, Special Publications*, **368**, 319-353.

Hock, R. (1999) A distributed temperature-index ice- and snowmelt model including potential direct solar radiation. *Journal of Glaciology*, **45**, 101-111.

Hornung, J.J., Asprion, U. and Winsemann, J. (2007) Jet-efflux deposits of a subaqueous ice-contact fan, glacial Lake Rinteln, northwestern Germany. Sedimentary Geology, **193**, 167–192.

Hoskin, C. and Burrell, D. (1972) Sediment transport and accumulation in a fjord basin, Glacier Bay, Alaska. *Journal of Geology*, **80**, 539-551.

IPCC, 2013. *Climate Change 2013: The Physical Science Basis*. WHO, UNEP.

Jakobsson, M., and 30 others (2012) The International Bathymetric Chart of the Arctic Ocean (IBCAO) Version 3.0. *Geophysical Research Letters*, **39**, doi:10.1029/2012GL052219.

Jirka, G. H. (2004) Integral model for turbulent buoyant jets in unbounded stratified flows. part 1: single round jet. *Environmental Fluid Mechanics*, *4*, 1–56.

Kehrl, L.M., Hawley, R.L., Powell, R.D. and Brigham-Grette, J. (2011) Glacimarine sedimentation processes at Kronebreen and Kongsvegen, Svalbard. *Journal of Glaciology*, **57**, 841-847.

Koch, Z.J. and Isbell, J.L. (2013) Processes and products of grounding-line fans from the Permian Pagoda Formation, Antarctica: insight into glacigenic conditions in polar Gondwana. *Gondwana Research*, **24**, 161-172.

Lane-Serff, G. F., and T. J. Moran (2005) Sedimentation from buoyant jets. *Journal of Hydraulic Engineering-ASCE*, **13**, 166–174.

Lang, J., Dixon, R.J., Le Heron, D.P. and Winsemann, J. (2012) Depositional architecture and sequence stratigraphic correlation of Upper Ordovician glaciogenic deposits, Illizi Basin, Algeria. In: Huuse, M., Redfern, J., Le Heron, D.P., Dixon, R.J., Moscariello, A. and Craig, J. (eds) Glaciogenic Reservoirs and Hydrocarbon Systems. *Geological Society, London, Special Publications*, **368**, 293-317

Le Heron, D.P. and Craig, J. (2008) First-order reconstructions of a Late Ordovician Saharan ice sheet. *Journal of the Geological Society, London*, **165**, 19-29.

Le Heron, D.P. and Dowdeswell, J.A. (2009) Calculating ice volumes andice flux to constrain the dimensions of a 440 Ma North African ice sheet. *Journal of the Geological Society, London*, **166**, 277-281.

Le Heron, D.P., Sutcliffe, O., Bourgig, K., Craig, J., Visentin, C and Whittington, R. (2004) Sedimentary architecture of Upper Ordovician tunnel valleys, Gargaf Arch, Libya: implications for the genesis of a hydrocarbon reservoir. *GeoArabia*, **9**, 171-176.

Livingstone, S.J., Ó Cofaigh, C., Stokes, C.R., Hillenbrand, C.-D., Vieli, A. and Jamieson, S.R., 2012. Antarctic palaeo-ice streams. *Earth-Science Reviews*, **111**, 90-128.

Lønne, I., Nemec, W. Blikra, L.H. and Lauritsen, T. (2001) Sedimentary architecture and dynamic stratigraphy of a marine ice-contact system. Journal of Sedimentary Research, **71**, 922-943.

McClure, H.A. (1978) Early Palaeozoic glaciation in Arabia. Palaeogeography, Palaeoclimatology, Palaeoecology, **25**, 315–326.

McMillan, M., Shepherd, A., Gourmelen, N., Dehecq, A., Leeson, A., Ridout, A., Flament, T., Hogg, A., Gilbert, L. Benham, T., van den Broeke, M., Dowdeswell, J.A., Fettweis, X. and Strozzi, T. (Submitted) Rapid dynamic activation of a marine-based Arctic ice cap. *Geophysical Research Letters*.

Meier, M.F. and Post, A. (1969) What are glacier surges? *Canadian Journal of Earth Sciences*, **6**, 807-817.

Moreau, J., Ghienne, J.-F., Le Heron, D., Rubino, J.-L. and Deynoux, M. (2005) A 440 Ma old ice stream in North Africa. *Geology*, **33**, 753–756.

Morton, B. (1959) Forced plumes. *Journal of Fluid Mechanics*, **5**, 151-163.

Mugford, R.I. and Dowdeswell, J.A. (2011) Modeling glacial meltwater plume dynamics and sedimentation in high-latitude fjords. *Journal of Geophysical Research*, **116**, doi:10.1029/2010JF001735.

Mulder, T. and Syvitski, J.P.M. (2005) Turbidity currents generated at river mouths during exceptional discharges to the world oceans. *Journal of Geology*, **103**, 285-299.

Ó Cofaigh, C., Pudsey, C.J., Dowdeswell, J.A. and Morris, P. (2002) Evolution of subglacial bedforms along a paleo-ice stream, Antarctic Peninsula continental shelf. *Geophysical Research Letters*, **29**, doi:10.1029/2001.GL014488.

Ó Cofaigh, C. (1996) Tunnel valley genesis. *Progress in Physical Geography*, **20**, 1-19.

Ottesen, D. and Dowdeswell, J.A. (2006) Assemblages of submarine landforms produced by tidewater glaciers in Svalbard. *Journal of Geophysical Research*, **111**, doi:10.1029/2005JF000330.

Pattyn, F. (2005) GRANTISM: An Excel model for Greenland and Antarctic ice-sheet response to climate change. *Computers and Geosciences,* **32,** 316-325.

Pelto, M.S. and Warren, C.R. (1991) Relationship between tidewater glacier calving velocity and water depth at the calving front. *Annals of Glaciology*, **15**, 115-118.

Pfirman, S.L. and Solheim, A. (1989) Subglacial meltwater discharge in the open-marine tidewater glacier environment: observations from Nordaustlandet, Svalbard archipelago. *Marine Geology*, **86**, 265-281.

Powell, R.D. (1990) Glacimarine processes at grounding-line fans and their growth to ice-contact deltas. *In* Dowdeswell, J.A. and Scourse, J.D., (Eds), Glacimarine Environments: Processes and Sediments, *Geological Society, London, Special Publications*, **53**, 53-73.

Powell, R.D. and Cooper, J.M. (2002) A glacial sequence stratigraphic model for temperate, glaciated continental shelves. In: Dowdeswell, J.A. and Ó Cofaigh, C. (eds.) Glacier-Influenced Sedimentation on High-Latitude Continental Marginns. Geological Society, London, Special Publications, **203**, 215-244.

Powell, R.D. and Domack, E. (1995) Moderrn glaciomarine environments. *In* Menzies, J., (Ed.), *Glacial Environments, vol. 1: Modern Glacial Environments: Processes, Dynamics and Sediments*, 445-486. Butterworth-Heinemann, Oxford.

Powell, R.D. and Molnia, B.F. (1989) Glacimarine sedimentary processes, facies and morphology of the south-southeast Alaska shelf and fjords. *Marine Geology*, **85**, 359-390.

Rees, W.G. (2013) *Physical Principles of Remote Sensing* (3rd Edition). Cambridge University Press.

Rignot, E., Jacobs, S., Mouginot, J. and Scheuchl, B. (2013) Ice-shelf melting around Antarctica. *Science*, **341**, 266-270.

Robinson, P. and Dowdeswell, J.A. (2011) Submarine landforms and the behavior of a surging ice cap since the Last Glacial Maximum: the open-marine setting of eastern Austfonna, Svalbard. *Marine Geology*, **286**, 82-94.

Russell, H.A.J. and Arnott, R.W.C. (2003) Hydraulic-jump and hyperconcentrated-flow deposits of a glacigenic subaqueous fan: Oak Ridges Moraine, Southern Ontario, Canada. Journal of Sedimentary Research, **73**, 887–905

Rye, C.J., Willis, I.C., Arnold, N.S. and Kohler, J. (2012) On the need for automated multi-objective optimization and uncertainty estimation of glacier mass balance models. *Journal of Geophysical Research*, **117**, doi:10.1029/2011JF002184.

Schuler, T.V., Loe, E., Taurisano, A., Eiken, T. Hagen, J.O. and Kohler, J. (2007) Calibrating a surface mass-balance model for Austfonna ice cap, Svalbard. *Annals of Glaciology*, **46**, 241-248.

Schytt, V. (19690 Some comments on glacier surges in eastern Svalbard. *Canadian Journal of Earth Sciences,* **6**, 867-871.

Scotese, C.R., Boucot, A.J. and McKerrow, W.S. (1999). Gondwana palaeogeography and palaeoclimatology. Journal of African Earth Sciences, **28**, 99–114.

Seramur, K.C., Powell, R.D. and Carlson, P.R. (1997) Evaluation of conditions along the grounding line of temperate marine glaciers: an example from Muir Inlet, Glacier Bay, Alaska. *Marine Geology*, **140**, 307-327.

Shreve, R.L. (1972) Movement of water in glaciers. *Journal of Glacio*logy, **11**, 205-214.

Solheim, A. (1991) The depositional environment of surging sub-polar tidewater glaciers: a case study from Nordaustlandet, northern Barents Sea. *Norsk Polarinstitutt Skrifter,* **194**, 97 pp.

Solheim, A. and Pfirman, S.L. (1985) Sea-floor morphology outside a grounded, surging glacier; Bråsvellbreen, Svalbard. *Marine Geology*, **65**, 127-143.

Sparks, R.S.J., Carey, S.N. and Sigurdsson, H. (1991) Sedimentation from gravity currents generated by turbulent plumes. *Sedimentology*, **38**, 839–856.

Stewart, M.A. and Lonergan, L. (2011) Seven glacial cycles in the middle-late Pleistocene of northwest Europe; geomorphic evidence from buried tunnel valleys. *Geology*, **39**, 283-286.

Syvitski, J.P.M. (1989) On the deposition of sediment within glacier-influenced fjords: oceanographic controls. *Marine Geo*logy, **85**, 301-329.

Taurisano, A., Schuler, T.V., Hagen, J.O., Eiken, T., Loe, E., Melvold, K. and Kohler, J. (2007) The distribution of snow accumulation across the Austfonna ice cap, Svalbard: direct measurements and modelling. *Polar Research*, **26**, 7-13.

Trusel, L.D., Powell, R.D., Cumpston, R.M. and Brigham-Grette, J. (2010) Modern glacimarine processes and potential future behaviour of Kronebreen and Kongsvegen polythermal tidewater glaciers, Kongsfjorden, Svalbard. *In* Howe, J.A., Austin, W.E.N., Forwick, M. and Paetzel, M., (Eds), Fjord Systems and Archives, *Geological Society, London, Special Publication*, **344**, 89-102.

Vaslet, D. (1990) Upper Ordovician glacial deposits in Saudi Arabia. Episodes, **13**, 147–161.

Winsemann, J., Hornung, J. J., Meinsen, J., Asprion, U., Polom, U., Brandes, C., Bussmann, M. and Weber, C. (2009) Anatomy of a subaqueous ice-contact fan and delta complex, Middle Pleistocene, NW Germany. *Sedimentology*, **56**, 1041–1076.

FIGURE CAPTIONS

Fig. 1. The Austfonna Ice Cap on Nordaustlandet, eastern Svalbard, with meltwater plumes along its marine margin (Bråsvelbreen to Leighbreen). (A) Ice-cap drainage basins (numbers) and ice divides for the ice cap are shown, from Dowdeswell (1986). Base image is a Landsat composite; VIC is Vestfonna Ice Cap. (B) Location of marine geophysical and geological data in Hartogbukta including ship's tracks (red) and sediment-core locations (black circles). Bathymetric contours every 25 m from IBCAO v. 3.0 (Jakobsson et al., 2012).

Fig. 2. (A) Methodology for plume identification from Landsat imagery (see text for details). (B) Photograph of a meltwater conduit at the margin of Basin 4 of Austfonna (Fig. 1B). Subglacial meltwater exits via a rounded tunnel, the top of which is visible above sea level. (C) Photograph of the boundary between brown, sediment-laden waters immediately offshore Austfonna in Hartogbukta (Fig. 1B) and clearer, blue ocean water in the foreground. Photographs: J.A. Dowdeswell.

Fig. 3. Meltwater plumes identified offshore Austfonna's marine margin. (A) All plumes observed from Landsat imagery spanning 1976-2012. Base image is Landsat MSS image 215/002 acquired on 23 July 2001. Aerial photographs showing sediment-laden meltwater plumes (arrowed) from (B) Basins 3 and 4, and (C) Basins 6 and 7. Aerial photographs acquired in 2011, courtesy of Norsk Polarinstitutt (NPI).

Fig. 4. Observations of meltwater plumes. (A) Plume observations by Plume Identification Number for each Landsat scene processed. (B) Frequency distribution diagram for observations of meltwater plumes; times when plumes were obscured (cloud, adjacent plumes) are not included; ice drainage basins are also shown.

Fig. 5. Changes in the position of the marine margin of Austfonna over a 40-year period from Landsat imagery. (A) Marine margin of Austfonna in summer 2011 with ice-margin positions for 1973 (red), 1981 (cyan), 1991 (yellow) and 2001 (white). (B), (C) and (D) show zoomed areas located in A. The underlying satellite imagery is composited from Landsat ETM+ scenes 211/002 and 211/003 of 27 August 2011 and 209/003 of 28 July 2011, with any remaining gaps filled by averaging of neighbouring values. (E) Average annual marine margin change for each drainage basin for the periods 1991-2001 and 2001-2011.

Fig. 6. Sensitivity tests of subglacial melt-model predictions of drainage beneath Austfonna varying the value of K (A-D), comparing drainage for the same day in a "cold" year (2001) and a "warm" year (2002) (E-F), and varying the amount of melt released from the snowpack into the basal water system (G-H). (A) Subglacial discharge using K = 0.25; (B) K = 0.5; (C) K = 0.75; (D) K = 1.0. (E) Subglacial discharge for 10 July 2001 with runoff to the bed if melt (M) > 0.3 times the snow depth (SD). (F) Subglacial discharge for 10 July 2002; runoff if M > 0.6SD. (G) Subglacial discharge for 10 July 2002; runoff if M > 0.3SD. (H) Subglacial discharge for 10 July 2002; runoff if M > 0.6SD. For A-D the colour scale is $\log_{10}$ of total water volume discharged, i.e. 8 = 100 000 000 m^3 of water (assuming 100 days gives 11.57 m^3 s^{-1} average discharge). For tests E-H, the colour scale shows $\log_{10}$ of the average diurnal discharge, in m^3s^{-1}, i.e. 2 = 100 m^3 s^{-1}.

Fig. 7. Model-predicted subglacial drainage pattern for early-, mid- and late-melt season dates on Austfonna compared with observed meltwater plumes on Landsat imagery from the same day. Model uses K = 5 in each case; scale is $\log_{10}$ of average diurnal discharge, i.e. 2 = 100 m^3 s^{-1}. (A) 10 July 2002. (B) 27 July 2006. (C) 5 August 2006. (D) 27 August 2011.

Fig. 8. Tabular comparison between the satellite-observed locations of meltwater plumes (from Fig. 4A), representing stream portals at the margins of Austfonna, and predictions from the numerical model of flow-routing for early-, mid- and late-melt season dates. (A) 10 July 2002. (B) 27 July 2006. (C) 5 August 2006. (D) 27 August 2011.

Fig. 9. *SedPlume* model sensitivity tests showing sediment deposition rate with distance from a glacier front beyond a melt-stream portal. Sensitivity tests varying: (A) Initial plume discharge; (B) Conduit radius; (C) Initial sediment concentration; and (D) Initial sand fraction. Apart from the parameter being varied in A-D initial inputs were: initial plume discharge = 80 m^3 s^{-1}; conduit radius = 5 m; initial sediment concentration = 100 mg l^{-1}; sand fraction at 320 m from glacier front = 13%. The initial sand fraction is the inverse, calculated from fractions of 5%, 13% and 18% at 320 m from the ice margin. This range was determined from grain-size fractions measured from core GC03 in Hartogbukta (Fig. 10).

Fig. 10. Marine sediments from Hartogbukta, eastern Nordaustlandet, Svalbard. (A) Grain-size data for sandy facies in cores GC02 and GC03 (located in Fig. 1B). The GC03 core site

was 320 m from the ice margin in 2006 when the core was acquired. (B) Core photograph of poorly sorted sandy facies with IRD in GC02; red star indicates grain size sample location.

Fig. 11. *SedPlume* model predictions of annual sediment deposition on an ice-proximal fan in summer 2006. (A) Time-series of plume discharge, Q, through 2006, calculated from an ice-cap surface melt model. (B) The accumulation of sediment with distance from the glacier is shown for June, July, August. (C) Plan-view of total thickness of sediment deposited over the year on the fan. (D) Total annual accumulation of sediment with distance from the glacier for 2006; also shown is calculated accumulation with Q of 10 and 100 times the 2006 result. Initial inputs for all three runs were: sand fraction at 320 m = 13%; initial sediment concentration = 50 mg l^{-1}; conduit radius = 5 m.

Fig. 12. Marine-geophysical data acquired in 2006 from Hartogbukta (Fig. 1B). (A) Multibeam bathymetry showing glacigenic deposits including a morainal bank complex (MBC) with possible ice-proximal fan (IPF) component (centre of image). Acquisition system: Kongsberg EM120; frequency 12 kHz; grid-cell size 10 m. (B) Line interpretation of landforms on the seafloor for part of A: recessional moraines (black), polygonal sediment deposits, sometimes streamlined (brown). Three moraines (light grey) and an IPF (dark grey) comprise the MBC. (C) TOPAS PS18 sub-bottom profile (vertical resolution 20 cm) over large moraine 1 with asymmetry indicating "push" by a stable or readvancing ice margin. (D) Sub-bottom profile over large moraine 2 and the IPF. Sub-bottom reflections (arrowed) indicate thicknesses for the moraine may exceed 30 m and fan thickness is 10-20 m.

Fig. 13. Schematic models and examples of ice-proximal deposits (IPDs) formed at marine-terminating ice margins experiencing different modes of ice advance/retreat. (A) Stable ice margin with melt-stream portal; sedimentation forms an ice-proximal fan (IPF). (B) Discrete IPDs or small fans actively building up offshore of Kronebreen, Kongsfjorden. Data courtesy of the Norwegian Hydrographic Service (permission No. 14/G754). Acquisition system: Kongsberg EM3002D; frequency 300 kHz; grid-cell size 5 m. (C) Quasi-stable ice margin producing a morainal bank complex (MBC). (D) MBC in Hartogbukta (Fig. 11), with morainal (M) and fan components (F). (E) A retreating ice margin with episodic and brief still-stands resulting in small IPDs (i) offshore plume locations. (F) Small IPDs (i) close to the grounding line in Hartogbukta; accumulations occur with ridges interpreted as recessional moraines (r).

Fig. 14. Architecture and sedimentary facies of ice-proximal fans (IPFs) and morainal bank complexes (MBCs) from Late Ordovician rocks of the Illizi Basin, Algeria. (A) Schematic depositional model beyond melt-stream portals on the margin of a Late Ordovician glacier in the Illizi Basin. IRD is iceberg-rafted debris. (B) Core photographs from the Illizi Basin illustrating sedimentary facies developed axially to IPFs. Coloured bars correspond to the facies shown in (A). (C) Schematic depositional model at and beyond MBCs remote from melt-stream portals on the margin of a Late Ordovician glacier in the Illizi Basin. (D) Core photographs from the Illizi Basin illustrating sedimentary facies developed axially to MBCs. Greyscale bars correspond to the facies shown in (C). Based on the models of Lønne et al. (2001), Powell and Cooper (2002), Russell and Arnott (2003), and Hornung et al. (2007).

Fig. 15. Initial numerical modelling of a Late Ordovician African ice sheet with results for "warm", "cool" and "colder" conditions for A and B. (A) Predicted sliding velocity of an ice stream along a profile from its crest to its northern margins. (B) Predicted mean summer meltwater discharge, Q, along a profile from the ice-sheet crest to its northern margins. (C) Plan-view of predicted meltwater discharge from ice crest to margin within ice-stream (I) and inter-ice stream (IS) regions. (D) Plan-view of predicted meltwater channel stability from ice crest to margin within ice-stream (S) and inter-ice stream (IS) regions.

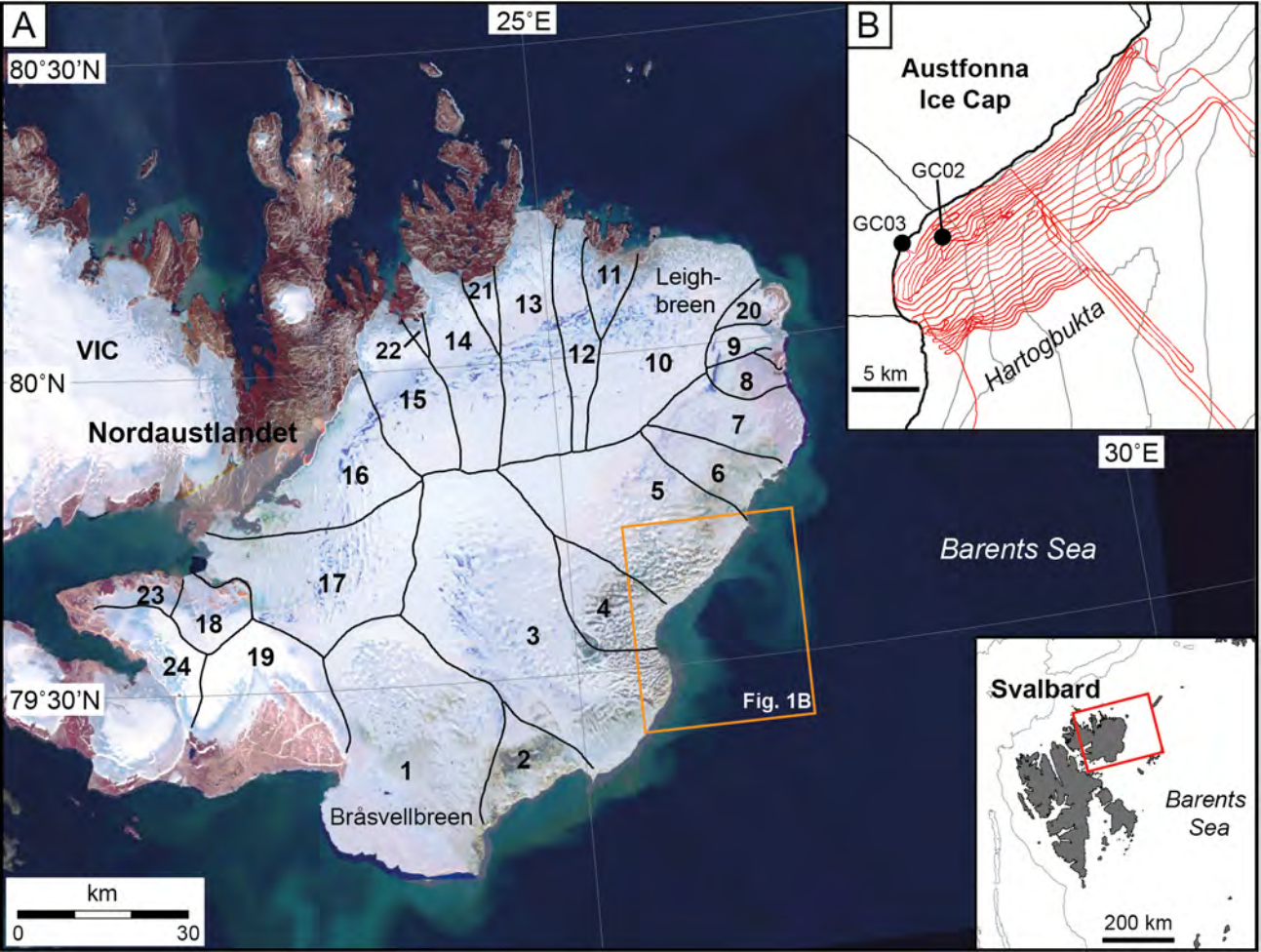
A
25°E
80°30'N
VIC
80°N
Nordaustlandet
Leigh-
breen
Barents Sea
30°E
79°30'N
Bråsvellbreen
Fig. 1B
1
2
3
4
5
6
7
8
9
10
11
12
13
14
15
16
17
18
19
20
21
22
23
24
km
0
30
B
Austfonna
Ice Cap
GC02
GC03
5 km
Hartogbukta
Svalbard
Barents
Sea
200 km

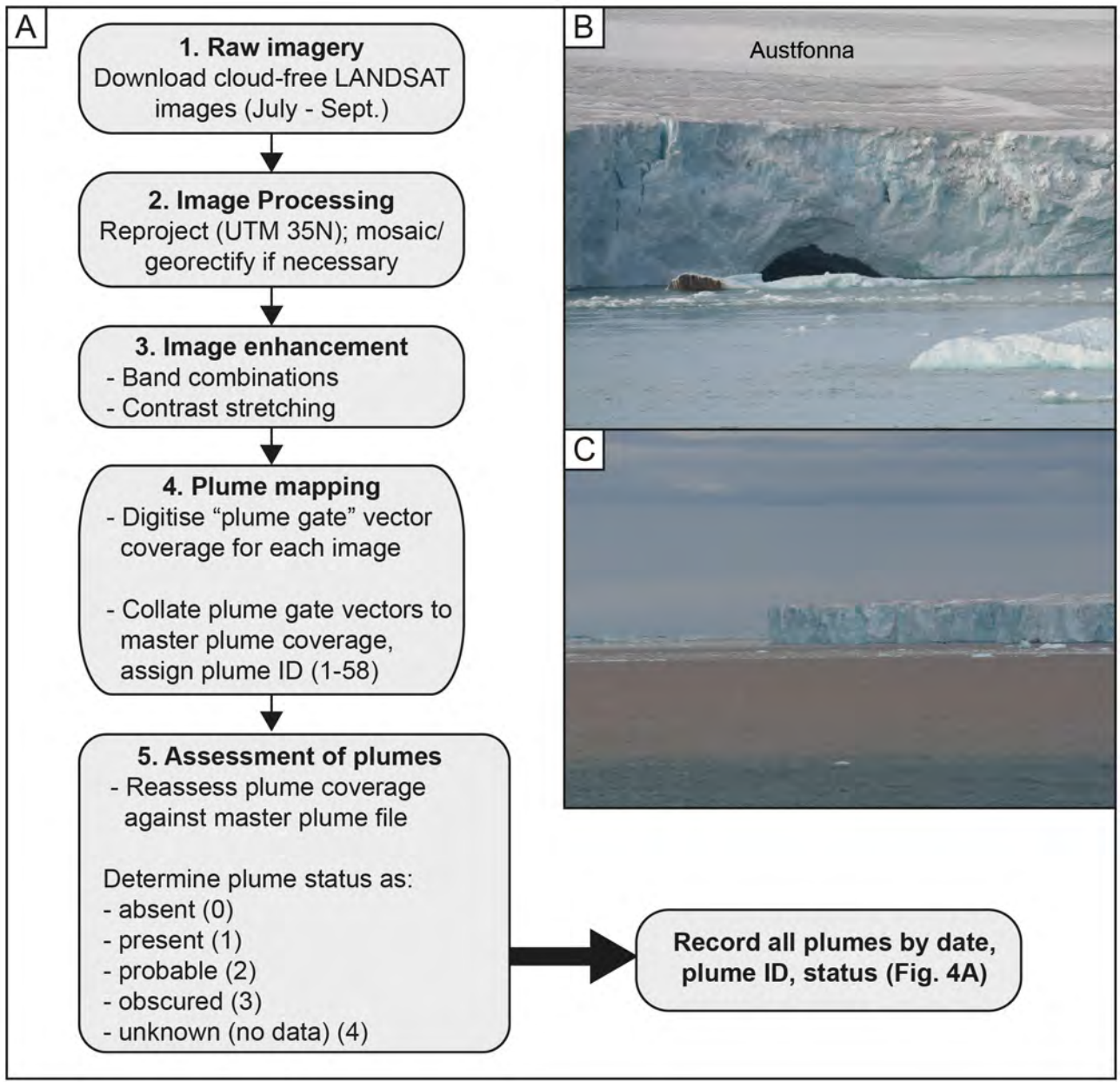
A
1. Raw imagery
Download cloud-free LANDSAT images (July - Sept.)
2. Image Processing
Reproject (UTM 35N); mosaic/ georectify if necessary
3. Image enhancement
- Band combinations
- Contrast stretching
4. Plume mapping
- Digitise "plume gate" vector coverage for each image
- Collate plume gate vectors to master plume coverage, assign plume ID (1-58)
5. Assessment of plumes
- Reassess plume coverage against master plume file
Determine plume status as:
- absent (0)
- present (1)
- probable (2)
- obscured (3)
- unknown (no data) (4)
Record all plumes by date, plume ID, status (Fig. 4A)
B
Austfonna
C

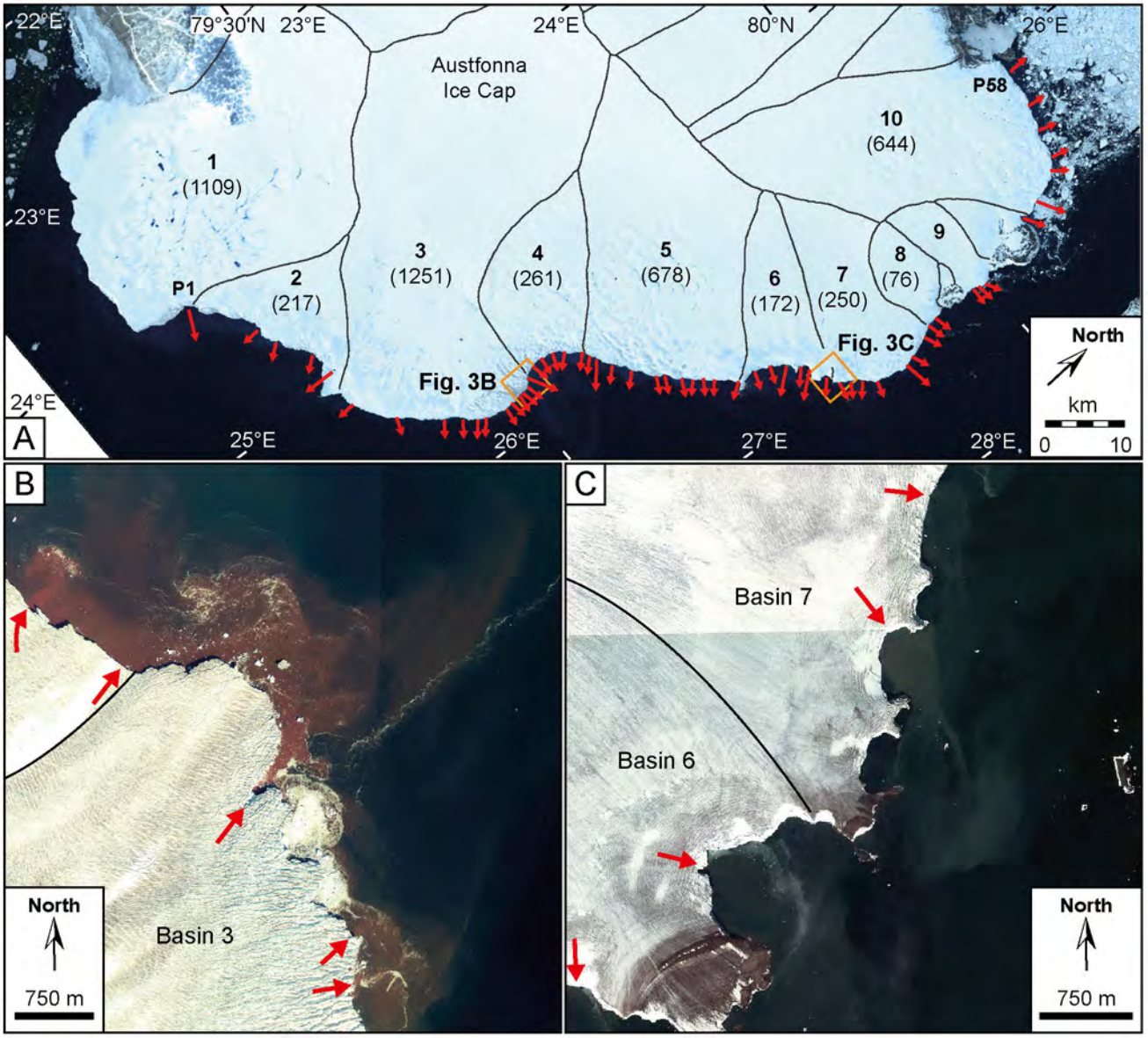
22°E
79°30'N
23°E
24°E
80°N
26°E
Austfonna
Ice Cap
P58
10
(644)
1
(1109)
23°E
9
8
(76)
3
(1251)
4
(261)
5
(678)
6
(172)
7
(250)
2
(217)
P1
Fig. 3C
Fig. 3B
North
km
0
10
24°E
A
25°E
26°E
27°E
28°E
B
Basin 3
North
750 m
C
Basin 7
Basin 6
North
750 m

Basin/ Plume ID / Landsat Acq. Date	Basin 2					Basin 3										Basin 4						Basin 5										Basin 6						Basin 7							B8		B9		Basin 10						
	1	2	3	4	5	6	7	8	9	10	11	12	13	14	15	16	17	18	19	20	21	22	23	24	25	26	27	28	29	30	31	32	33	34	35	36	37	38	39	40	41	42	43	44	45	46	47	48	49	50	51	52	53	54	55	56	57	58
14 July 1976																																																									
16 July 1976																																																								
23 July 1976																																																								
3 Aug. 1976																																																							
1 Aug. 1981																																																							
6 Sept. 1988																																																							
23 July 1991																																																							
15 Aug. 1993																																																							
19 July 2000																																																							
24 June 2001																																																							
10 July 2001																																																							
1 July 2002																																																							
8 July 2002																																																							
10 July 2002																																																							
12 July 2002																																																							
11 July 2004																																																							
31 July 2004																																																							
8 July 2005																																																							
30 July 2005																																																							
9 July 2006																																																							
11 July 2006																																																							
18 July 2006																																																							
23 July 2006																																																							
26 July 2006																																																							
27 July 2006																																																							
5 Aug. 2006																																																							
10 Aug. 2006																																																							
15 July 2007																																																							
1 July 2010																																																							
7 July 2010																																																							
21 July 2010																																																							
22 July 2010																																																							
25 July 2010																																																							
30 July 2010																																																							
4 Aug. 2010																																																							
10 Aug. 2010																																																							
19 Aug. 2010																																																							
20 Aug. 2010																																																							
12 Sept. 2010																																																							
28 July 2011																																																							
27 Aug. 2011																																																							
12 July 2012																																																							

Legend:

- Plume absent (0)
- Plume present (1)
- Probable plume (2)
- Blank = Obscured ice margin (3)
- No image available (4)

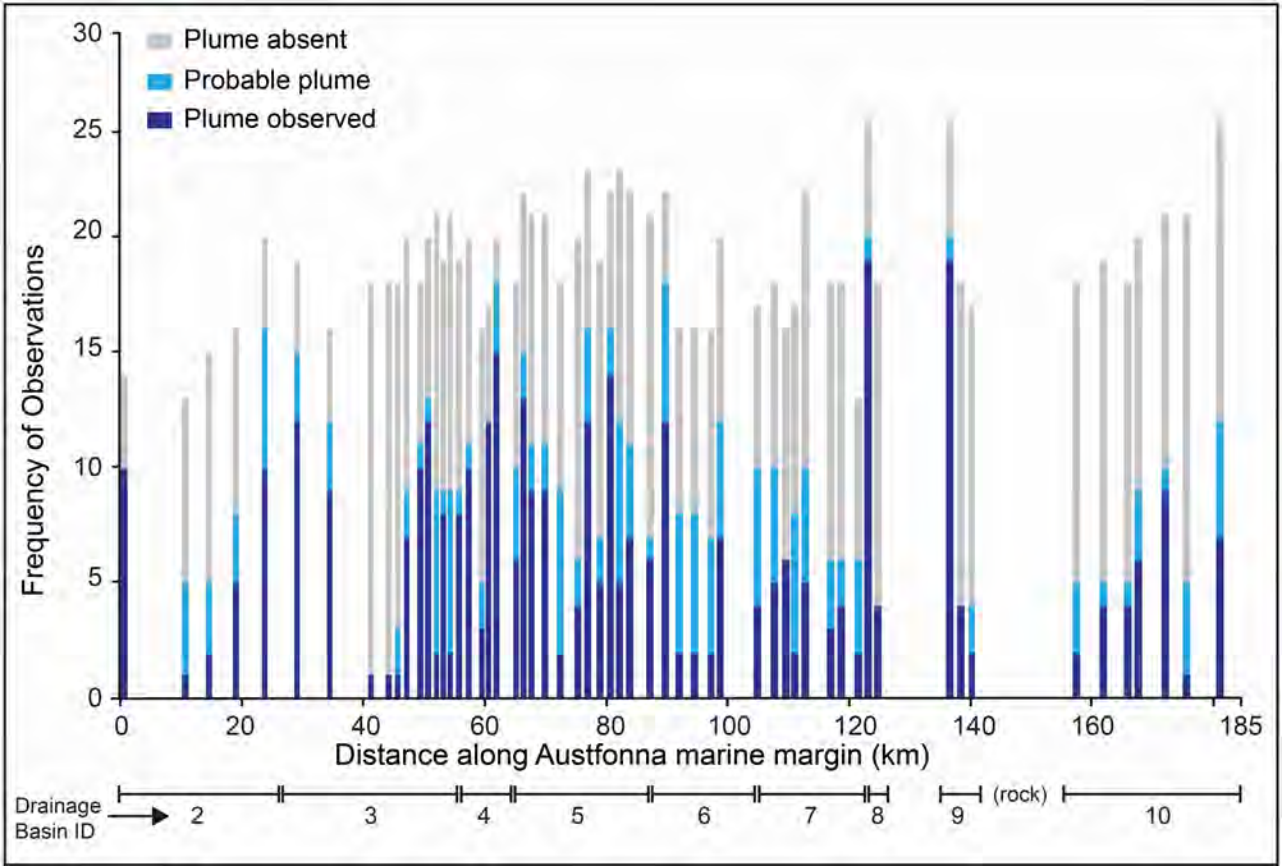
Plume absent
Probable plume
Plume observed
Frequency of Observations
30
25
20
15
10
5
0
0
20
40
60
80
100
120
140
160
185
Distance along Austfonna marine margin (km)
Drainage Basin ID
2
3
4
5
6
7
8
9
(rock)
10

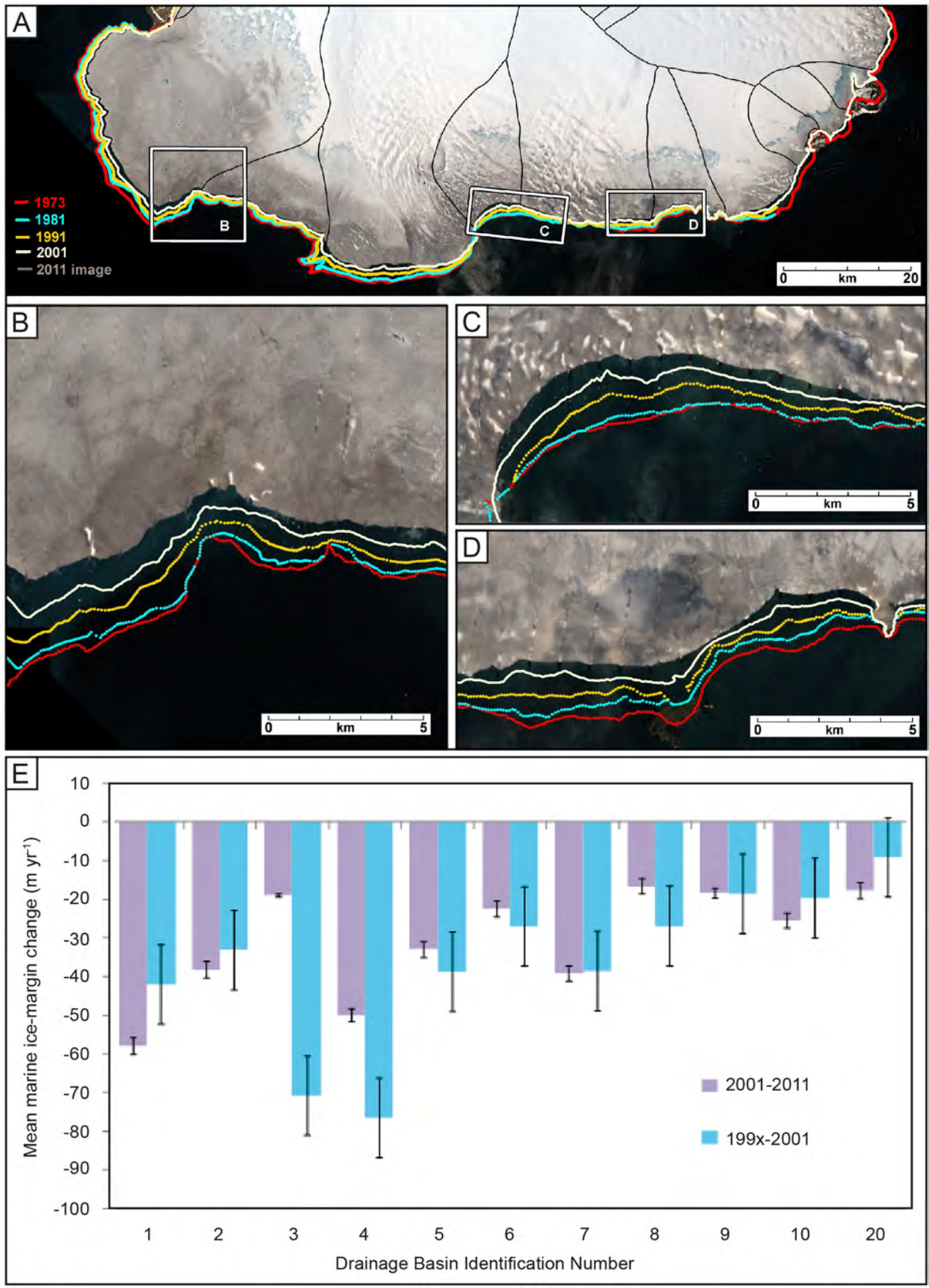
A
1973
1981
1991
2001
2011 image
B
C
D
0 km 20
B
0 km 5
C
0 km 5
D
0 km 5
E
Mean marine ice-margin change (m yr-1)
10
0
-10
-20
-30
-40
-50
-60
-70
-80
-90
-100
2001-2011
199x-2001
1
2
3
4
5
6
7
8
9
10
20
Drainage Basin Identification Number

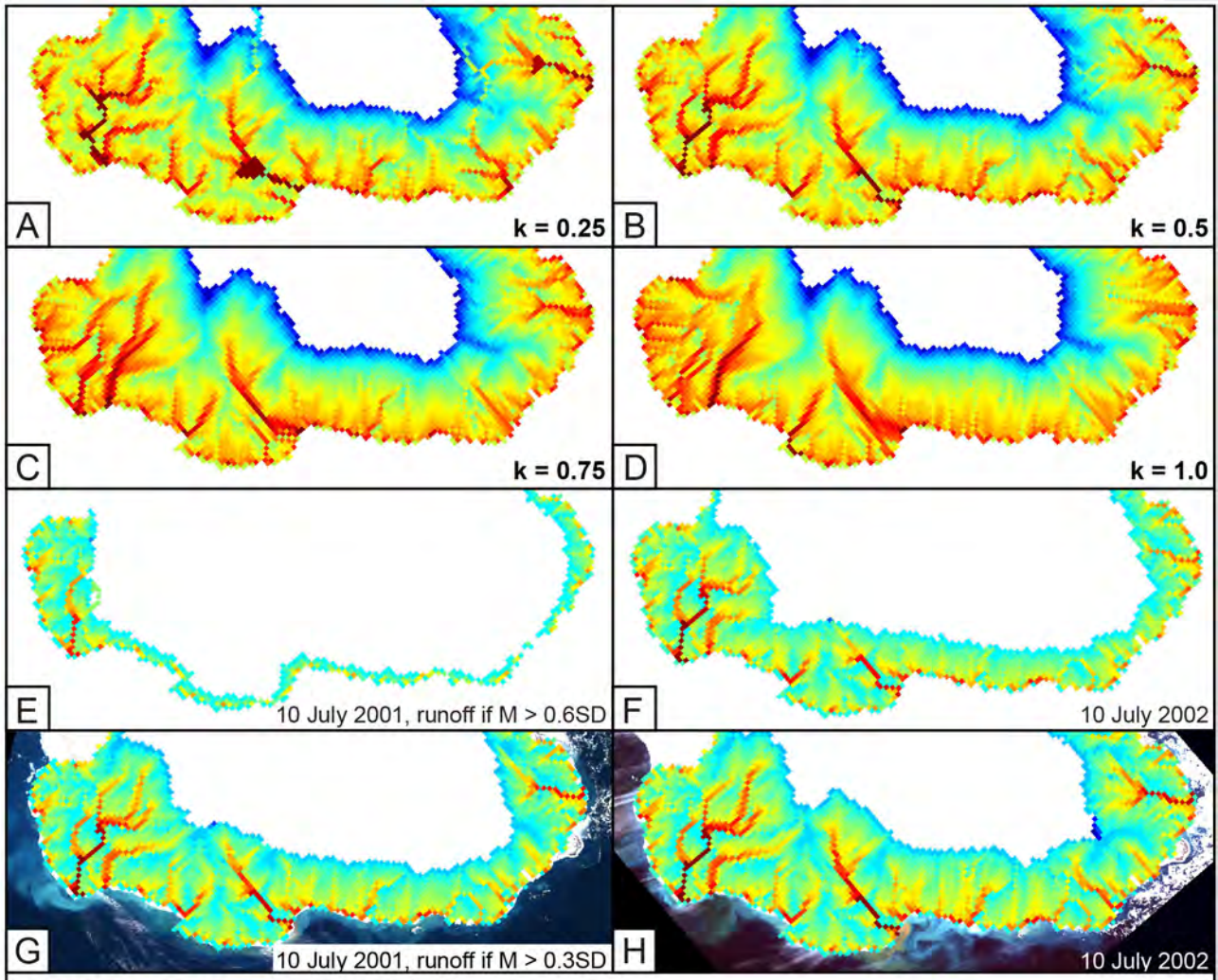
A
k = 0.25
B
k = 0.5
C
k = 0.75
D
k = 1.0
E
10 July 2001, runoff if M > 0.6SD
F
10 July 2002
G
10 July 2001, runoff if M > 0.3SD
H
10 July 2002
Legend for modelled discharge, Q (m³ s⁻¹):
For A-D colour scale is log10 of total water volume:
4
5
6
7
8
Q m³s⁻¹
For E-H colour scale:
-2
-1
0
1
2
Q m³s⁻¹

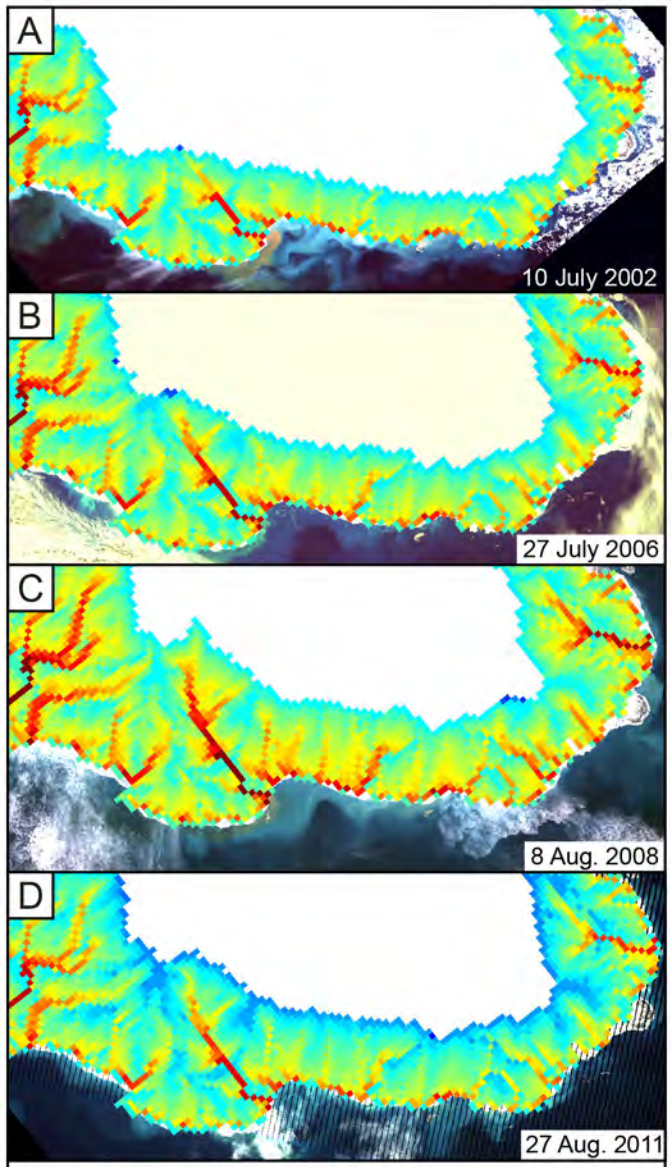
A
10 July 2002
B
27 July 2006
C
8 Aug. 2008
D
27 Aug. 2011
Legend for modelled discharge, Q:
-2
-1
0
1
2
Q
m3s-1

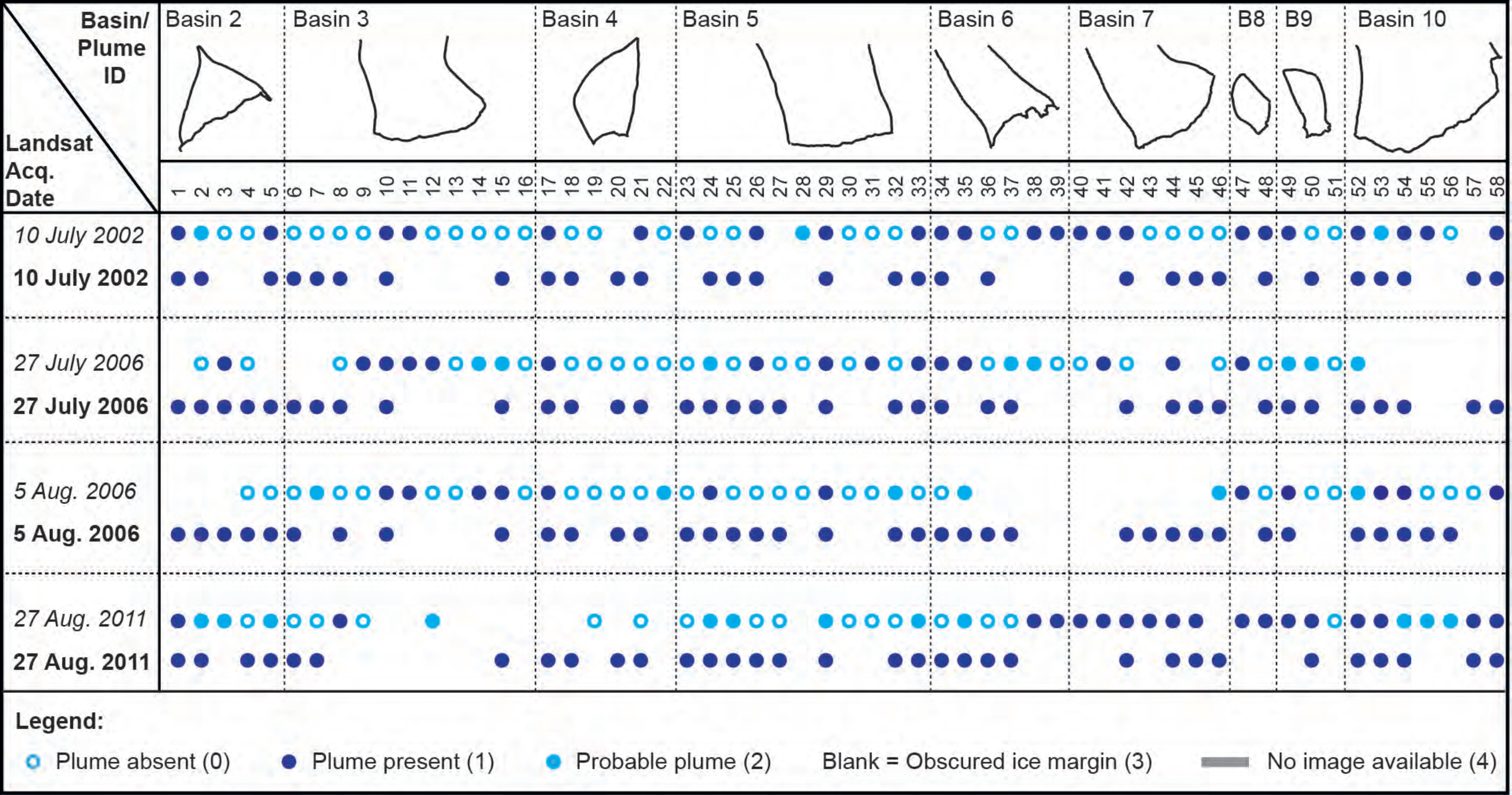
Basin/ Plume ID
Landsat Acq. Date
Basin 2
Basin 3
Basin 4
Basin 5
Basin 6
Basin 7
B8
B9
Basin 10
1 2 3 4 5 6 7 8 9 10 11 12 13 14 15 16 17 18 19 20 21 22 23 24 25 26 27 28 29 30 31 32 33 34 35 36 37 38 39 40 41 42 43 44 45 46 47 48 49 50 51 52 53 54 55 56 57 58
10 July 2002
10 July 2002
27 July 2006
27 July 2006
5 Aug. 2006
5 Aug. 2006
27 Aug. 2011
27 Aug. 2011
Legend:
Plume absent (0)
Plume present (1)
Probable plume (2)
Blank = Obscured ice margin (3)
No image available (4)

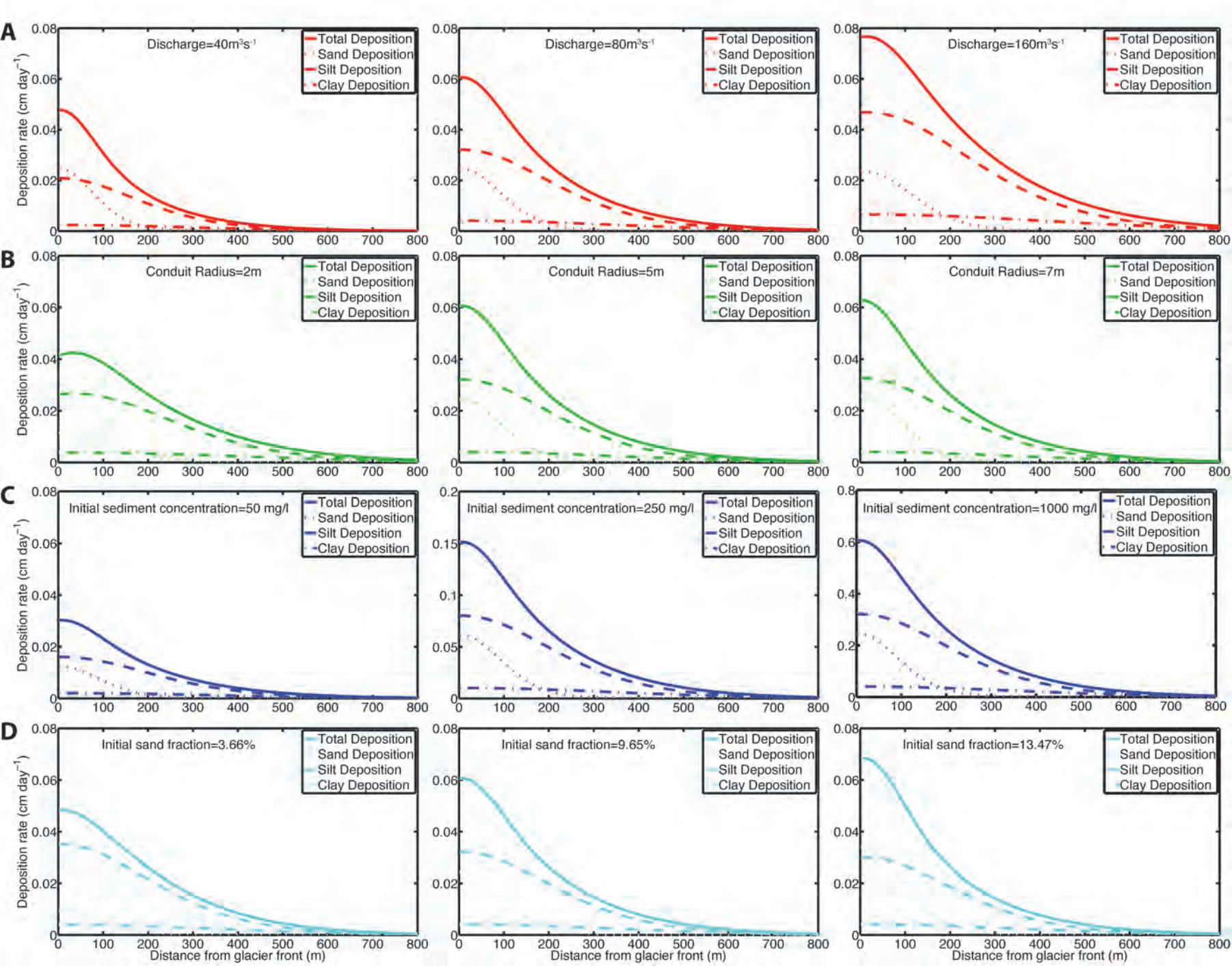
A
Discharge=40m3s-1
Discharge=80m3s-1
Discharge=160m3s-1
B
Conduit Radius=2m
Conduit Radius=5m
Conduit Radius=7m
C
Initial sediment concentration=50 mg/l
Initial sediment concentration=250 mg/l
Initial sediment concentration=1000 mg/l
D
Initial sand fraction=3.66%
Initial sand fraction=9.65%
Initial sand fraction=13.47%
Total Deposition
Sand Deposition
Silt Deposition
Clay Deposition
Deposition rate (cm day-1)
Distance from glacier front (m)

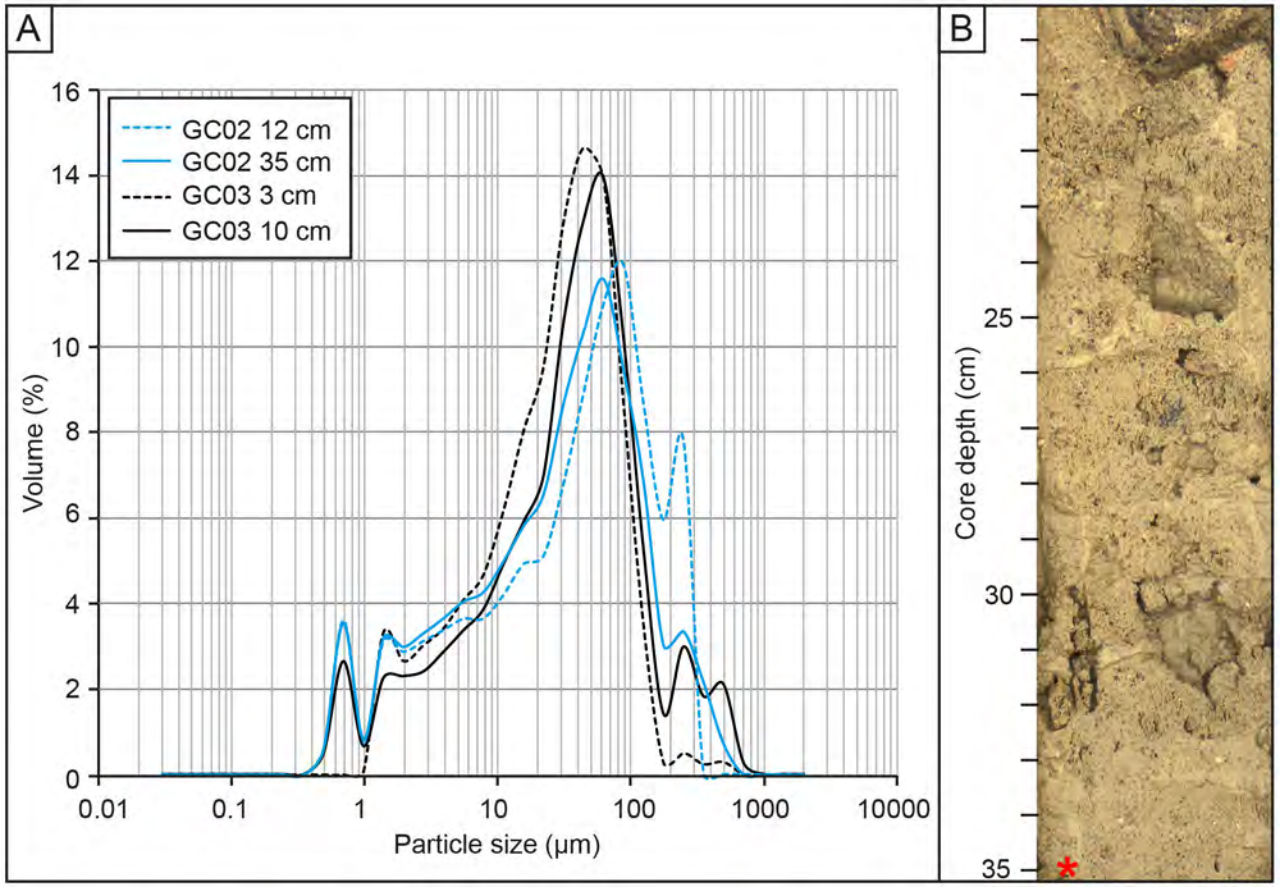
A
B
GC02 12 cm
GC02 35 cm
GC03 3 cm
GC03 10 cm
Volume (%)
Particle size (µm)
Core depth (cm)
0
2
4
6
8
10
12
14
16
0.01
0.1
1
10
100
1000
10000
25
30
35

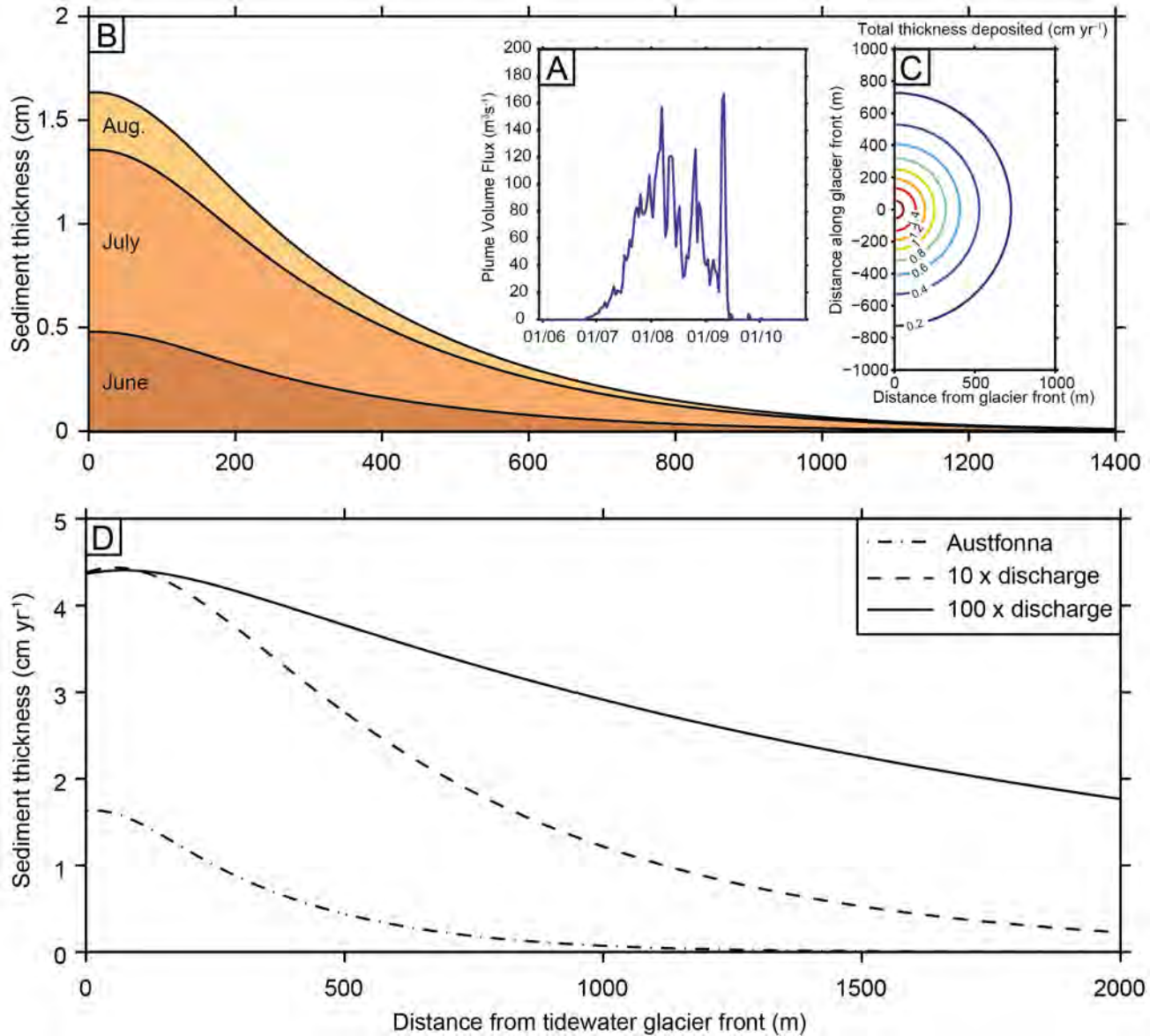
B
Aug.
July
June
Sediment thickness (cm)
A
Plume Volume Flux (m³s⁻¹)
01/06
01/07
01/08
01/09
01/10
C
Total thickness deposited (cm yr⁻¹)
Distance along glacier front (m)
Distance from glacier front (m)
D
Austfonna
10 x discharge
100 x discharge
Sediment thickness (cm yr⁻¹)
Distance from tidewater glacier front (m)

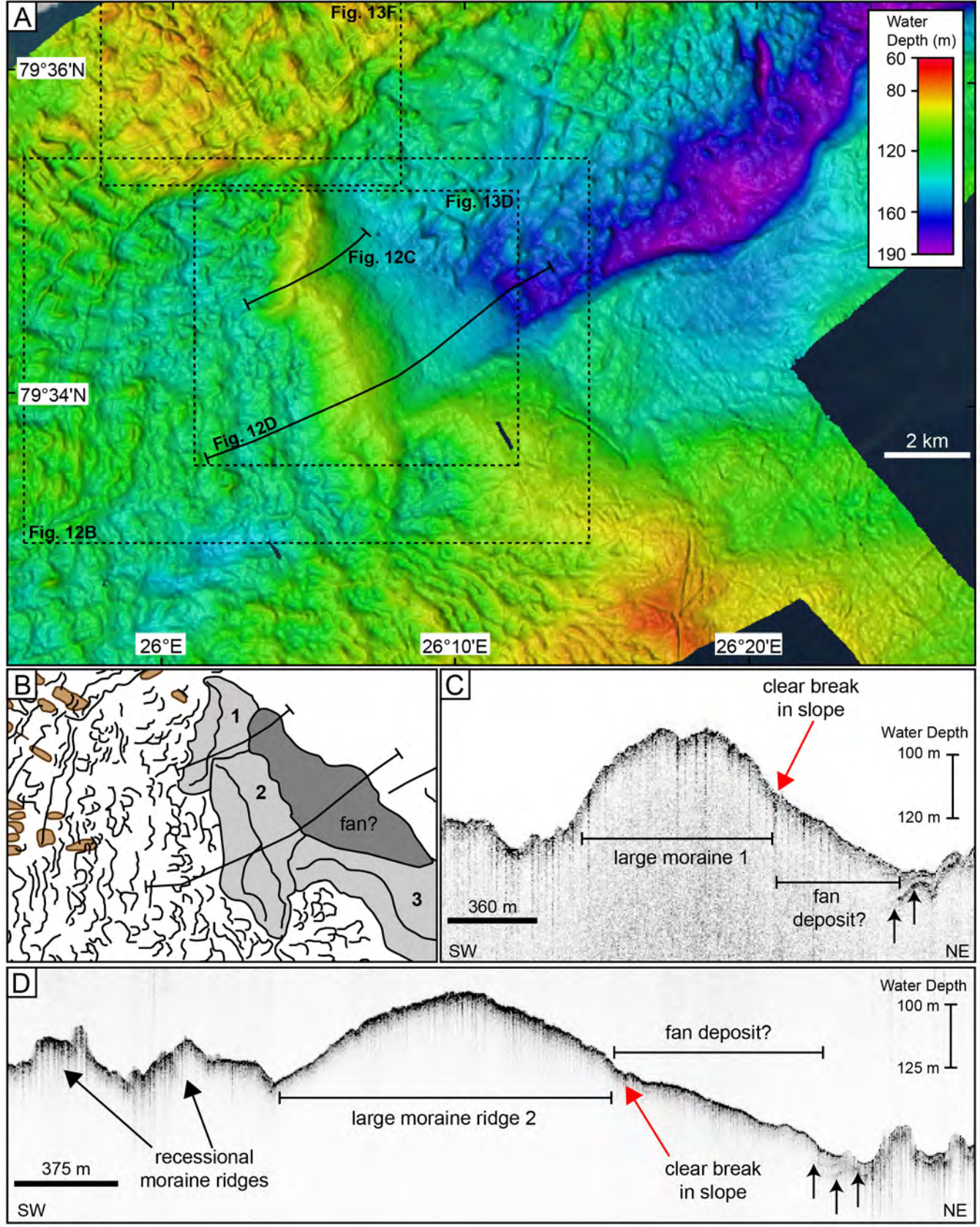
A
Fig. 13F
79°36'N
Fig. 13D
Fig. 12C
79°34'N
Fig. 12D
Fig. 12B
Water Depth (m)
60
80
120
160
190
2 km
26°E
26°10'E
26°20'E
B
1
2
fan?
3
C
clear break in slope
Water Depth
100 m
120 m
large moraine 1
fan deposit?
360 m
SW
NE
D
Water Depth
100 m
125 m
fan deposit?
large moraine ridge 2
375 m
recessional moraine ridges
clear break in slope
SW
NE

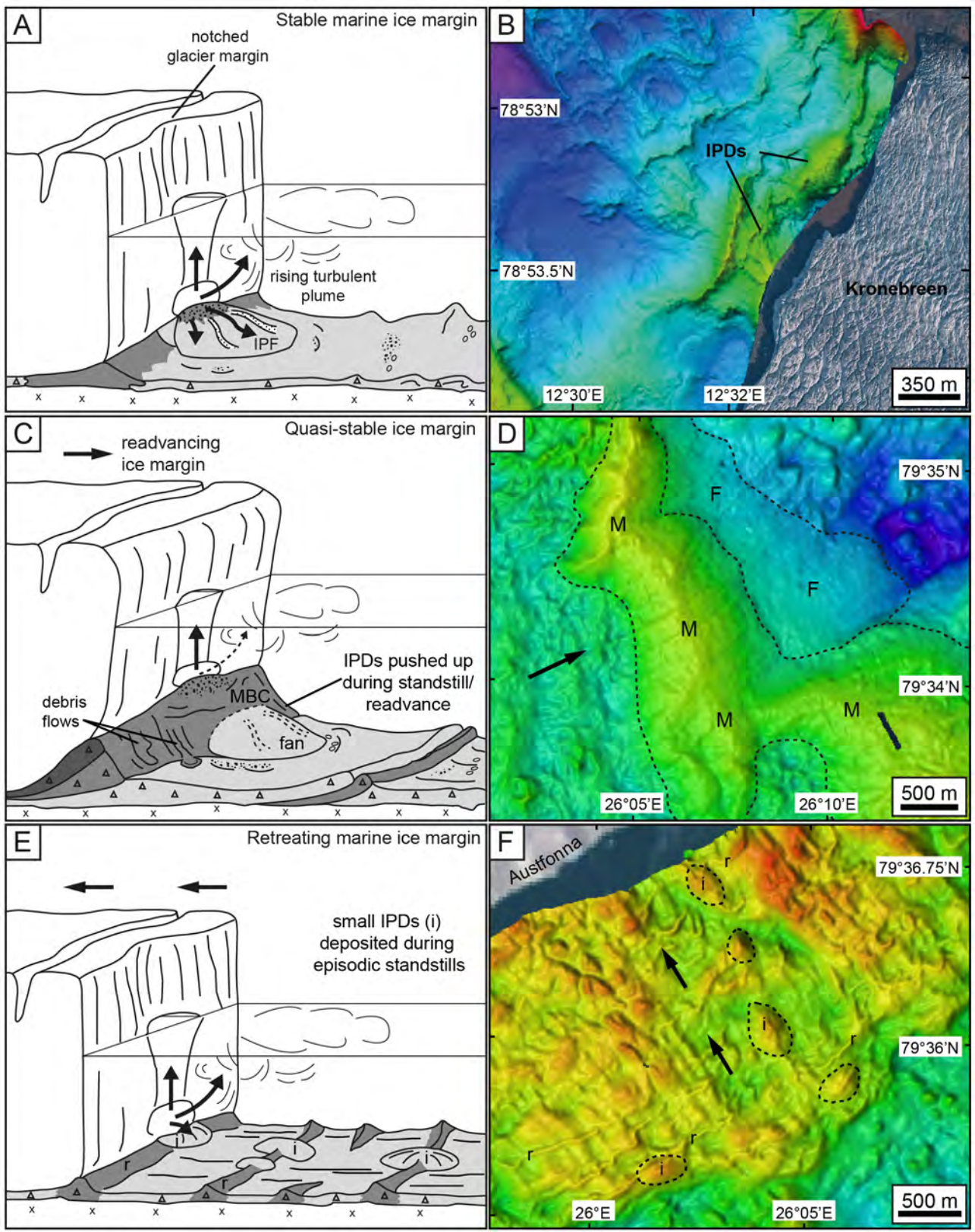
A
Stable marine ice margin
notched
glacier margin
rising turbulent
plume
IPF
B
78°53'N
IPDs
78°53.5'N
Kronebreen
12°30'E
12°32'E
350 m
C
Quasi-stable ice margin
readvancing
ice margin
IPDs pushed up
during standstill/
readvance
MBC
debris
flows
fan
D
79°35'N
F
M
F
M
79°34'N
M
M
26°05'E
26°10'E
500 m
E
Retreating marine ice margin
small IPDs (i)
deposited during
episodic standstills
i
r
F
Austfonna
79°36.75'N
79°36'N
26°E
26°05'E
500 m

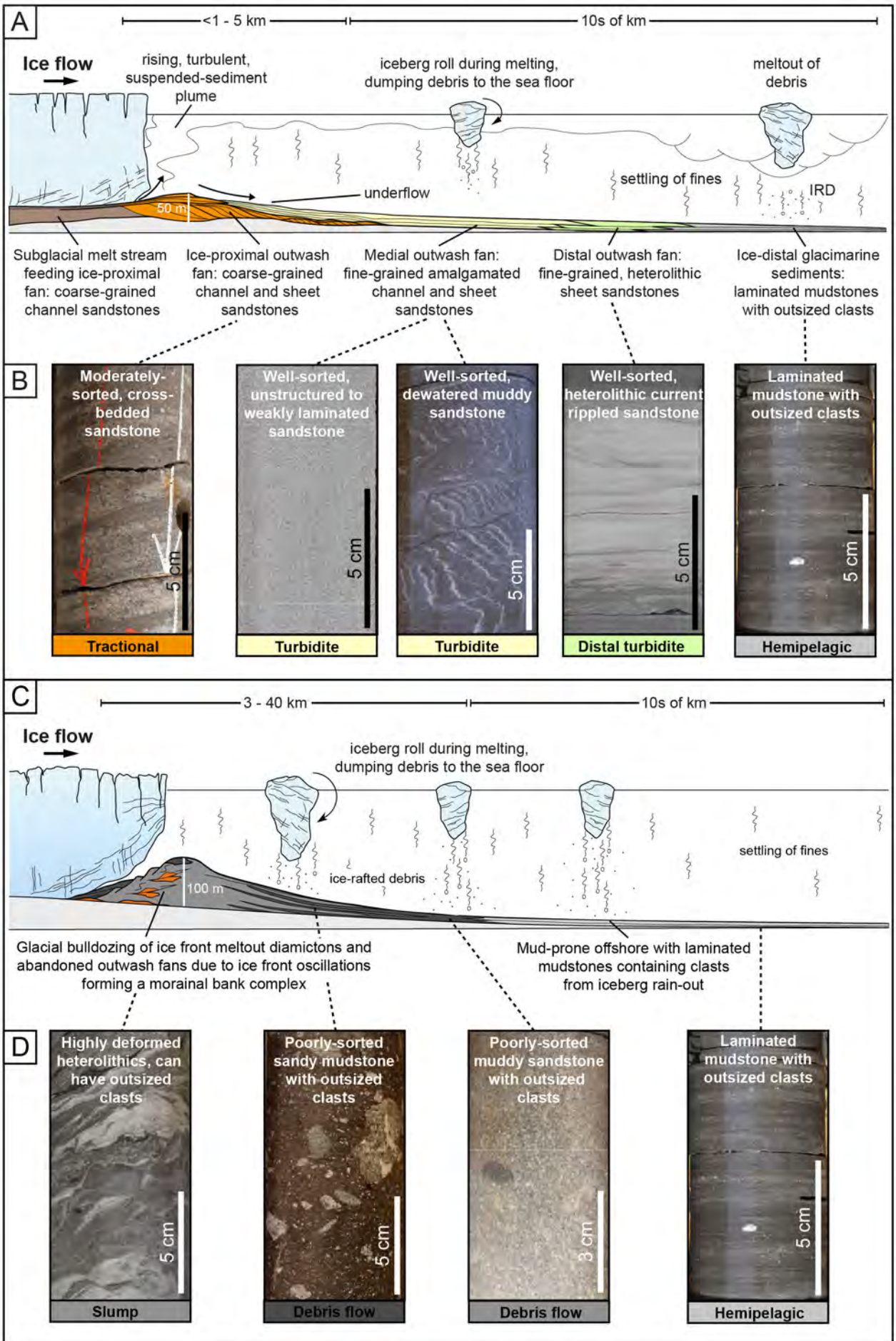
A
<1 - 5 km
10s of km
Ice flow
rising, turbulent, suspended-sediment plume
iceberg roll during melting, dumping debris to the sea floor
meltout of debris
settling of fines
IRD
underflow
50 m
Subglacial melt stream feeding ice-proximal fan: coarse-grained channel sandstones
Ice-proximal outwash fan: coarse-grained channel and sheet sandstones
Medial outwash fan: fine-grained amalgamated channel and sheet sandstones
Distal outwash fan: fine-grained, heterolithic sheet sandstones
Ice-distal glacimarine sediments: laminated mudstones with outsized clasts
B
Moderately-sorted, cross-bedded sandstone
5 cm
Tractional
Well-sorted, unstructured to weakly laminated sandstone
5 cm
Turbidite
Well-sorted, dewatered muddy sandstone
5 cm
Turbidite
Well-sorted, heterolithic current rippled sandstone
5 cm
Distal turbidite
Laminated mudstone with outsized clasts
5 cm
Hemipelagic
C
3 - 40 km
10s of km
Ice flow
iceberg roll during melting, dumping debris to the sea floor
settling of fines
ice-rafted debris
100 m
Glacial bulldozing of ice front meltout diamictons and abandoned outwash fans due to ice front oscillations forming a morainal bank complex
Mud-prone offshore with laminated mudstones containing clasts from iceberg rain-out
D
Highly deformed heterolithics, can have outsized clasts
5 cm
Slump
Poorly-sorted sandy mudstone with outsized clasts
5 cm
Debris flow
Poorly-sorted muddy sandstone with outsized clasts
3 cm
Debris flow
Laminated mudstone with outsized clasts
5 cm
Hemipelagic

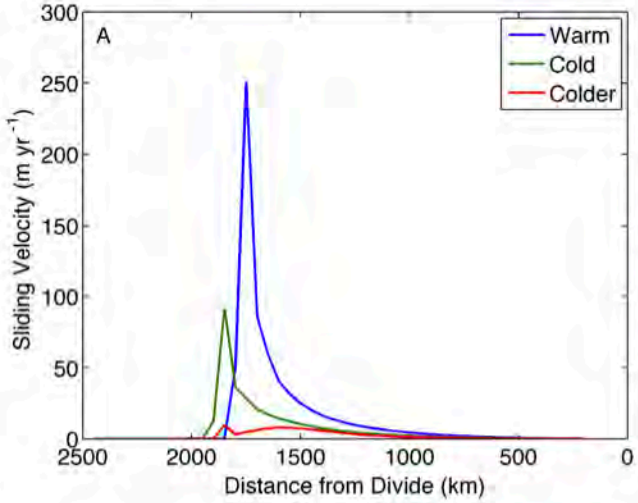
A
Warm
Cold
Colder
Sliding Velocity (m yr^{-1})
Distance from Divide (km)

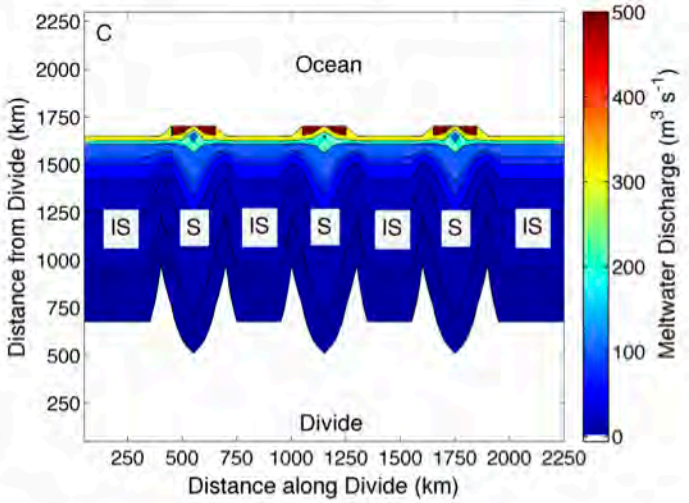
C
Ocean
Divide
IS
S
Distance from Divide (km)
Distance along Divide (km)
Meltwater Discharge (m^3 s^{-1})

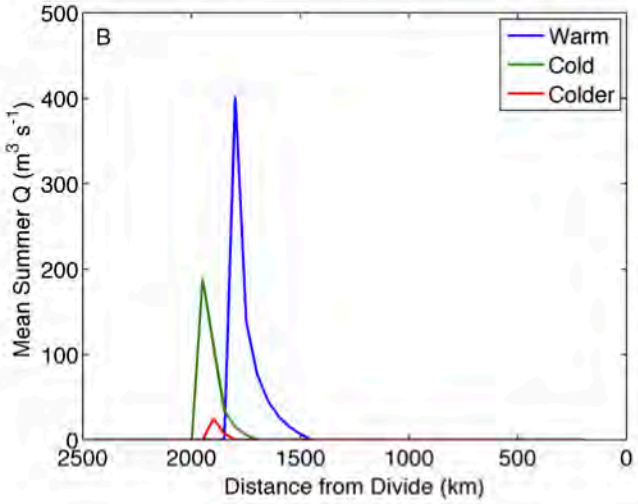
B
Warm
Cold
Colder
Mean Summer Q (m^3 s^{-1})
Distance from Divide (km)

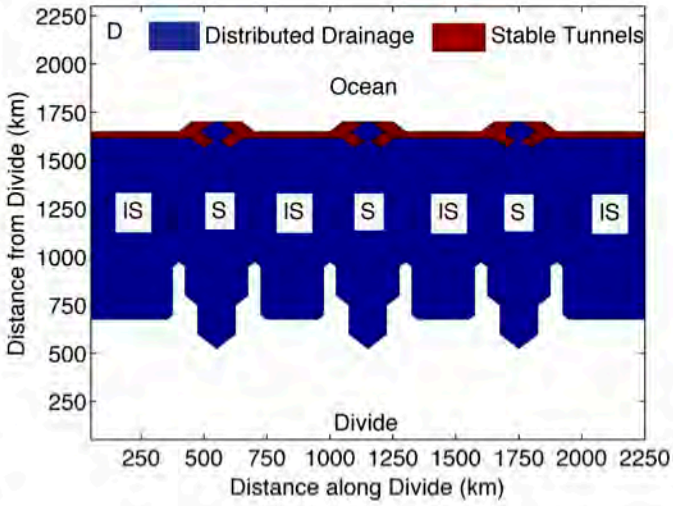
D
Distributed Drainage
Stable Tunnels
Ocean
Divide
IS
S
Distance from Divide (km)
Distance along Divide (km)